AFRL-RH-WP-TR-2017-0080

MATHEMATICAL MODEL OF HIF-1α PATHWAY, OXYGEN TRANSPORT AND HYPOXIA

Peter J. Robinson
C. Eric Hack

Henry M. Jackson Foundation
For the Advancement of Military Medicine
Wright-Patterson AFB OH

Elaine A. Merrill
David R. Mattie

Bioeffects Division
Molecular Bioeffects Branch

September 2017

Interim Report

Molecular Bioeffects Branch
Bioeffects Division
Airmen Systems Directorate
711th Human Performance Wing
Air Force Research Laboratory
Wright-Patterson AFB OH 45433-5707

NOTICE AND SIGNATURE PAGE

Using Government drawings, specifications, or other data included in this document for any purpose other than Government procurement does not in any way obligate the U.S. Government. The fact that the Government formulated or supplied the drawings, specifications, or other data does not license the holder or any other person or corporation; or convey any rights or permission to manufacture, use, or sell any patented invention that may relate to them.

This report was cleared for public release by the 88th ABW Public Affairs Office and is available to the general public, including foreign nationals. Copies may be obtained from the Defense Technical Information Center (DTIC) (http://www.dtic.mil).

Mathematical Model of HIF-1α Pathway, Oxygen Transport and Hypoxia

(AFRL-RH-WP-TR-2017-0080) has been reviewed and is approved for publication in accordance with assigned distribution statement.

MATTIE.DAVID.R.1230101880
Digitally signed by MATTIE.DAVID.R.1230101880
Date: 2017.12.05 12:29:15 -05'00'

DAVID R. MATTIE
Work Unit Manager
Molecular Bioeffects Branch

MILLER.STEPHANIE.A.1230536283
Digitally signed by MILLER.STEPHANIE.A.1230536283
Date: 2017.12.05 18:37:36 -06'00'

STEPHANIE A. MILLER, DR-IV, DAF
Chief, Bioeffects Division
Airman Systems Directorate
711th Human Performance Wing
Air Force Research Laboratory

This report is published in the interest of scientific and technical information exchange, and its publication does not constitute the Government's approval or disapproval of its ideas or findings.

REPORT DOCUMENTATION PAGE

Form Approved
OMB No. 0704-0188

1. REPORT DATE *(DD-MM-YYYY)*	2. REPORT TYPE	3. DATES COVERED *(From - To)*
20-09-2017	Interim	Oct 2016 – Sep 2017

4. TITLE AND SUBTITLE
Mathematical Model of HIF-1α Pathway, Oxygen Transport and Hypoxia

5a. CONTRACT NUMBER
In-House

5b. GRANT NUMBER
NA

5c. PROGRAM ELEMENT NUMBER
62202F

6. AUTHOR(S)
Robinson, Peter J.[1], Hack, C. Eric[1], Merrill, Elaine A.*, Mattie, David R.*

5d. PROJECT NUMBER
7757

5e. TASK NUMBER
HD

5f. WORK UNIT NUMBER
05/H0D1

7. PERFORMING ORGANIZATION NAME(S) AND ADDRESS(ES)
[1]HJF, 2728 Q St, Bldg 837, WPAFB OH 45433-5707

8. PERFORMING ORGANIZATION REPORT NUMBER

9. SPONSORING/MONITORING AGENCY NAME(S) AND ADDRESS(ES)
Air Force Materiel Command*
Air Force Research Laboratory
711th Human Performance Wing
Human Effectiveness Directorate
Bioeffects Division
Molecular Bioeffects Branch
Wright-Patterson AFB OH 45433-5707

10. SPONSOR/MONITOR'S ACRONYM(S)
711 HPW/RHDJ

11. SPONSORING/MONITORING AGENCY REPORT NUMBER
AFRL-RH-WP-TR-2017-0080

12. DISTRIBUTION AVAILABILITY STATEMENT
Distribution A: Approved for public release; distribution unlimited. (PA Case No. 88ABW-2017-6197, 11 Dec 2017)

13. SUPPLEMENTARY NOTES

14. ABSTRACT
Episodes of hypoxia-like events experienced by F-22 pilots after training missions have raised questions about pilot exposures and diminished operational mission accomplishment. These episodes identified data gaps in the understanding of pilot exposures in high performance aircraft. We, therefore, need to understand how levels of low oxygen at lower than atmospheric pressure causes physiological hypoxia, and how this relates to alterations in cognition. Oxygen sensing pathways, particularly those involving the oxygen sensing cytosolic gene transcription factor HIF-1α, are key to understanding these responses. A mathematical model was developed to integrate these experimental measurements and provide a description of hypoxia mechanisms and the organism's response. The initial iteration of our model focuses on oxygen delivery to the brain. It includes delivery of oxygen to the blood via hemoglobin binding, breathing rate and cardiac output, delivery of oxygen from the blood to the brain tissue, and the response of the HIF-1α signaling pathway in terms of alterations in gene expression and other brain tissue end-points. The model simulates time courses of brain oxygen, intracellular HIF-1α, transport to the nucleus, binding to hypoxia responsive element (HRE), and generation of transcription signal under altered blood oxygen levels. The HIF-1α model is partially parameterized based on experimental data in the literature. The model has been fitted to steady-state dose/response literature data for vascular endothelial growth factor (VEGF) and VEGF mRNA. The model also describes angiogenesis data, a process involving longer term changes in capillary densities in response to prolonged hypoxia exposures, while assuming linearity of dose/response for gene transcription process.

15. SUBJECT TERMS
mathematical model, signaling pathways, brain hypoxia, oxygen delivery, VEGF, angiogenesis, carotid body

16. SECURITY CLASSIFICATION OF:			17. LIMITATION OF ABSTRACT	18. NUMBER OF PAGES	19a. NAME OF RESPONSIBLE PERSON
U					D.R. Mattie
a. REPORT	b. ABSTRACT	c. THIS PAGE	SAR	49	19b. TELEPONE NUMBER (*Include area code)*
U	U	U			NA

Standard Form 298 (Rev. 8-98)
Prescribed by ANSI-Std Z39-18

THIS PAGE INTENTIONALLY LEFT BLANK.

TABLE OF CONTENTS

1.0 Summary 1
2.0 Introduction 2
2.1 Background 2
2.2 Oxygen Transport to Tissues 4
2.3 HIF-1α Pathway 6
2.4 Summary of Existing Mathematical Models 8
3.0 Methods 8
3.1 Oxygen Delivery Model 8
3.2 HIF-1α Mathematical Model for Brain 11
3.3 Parameter Values 13
3.4 Integrating the Oxygen Transport and HIF-1α Models 14
4.0 Results 14
4.1 Time-Course Simulations 14
4.2 Dose-Response Simulations 16
5.0 Conclusions and Future Work 17
5.1 Gene Transcription and Longer Term Effects 17
5.2 Capillary Densities and Angiogenesis 18
5.3 Inflammation 19
5.4 Carotid Body and Other Issues 22
6.0 References 24

Appendix A. Model Code: Combined Oxygen Transport and HIF-1α Model 28
Appendix B. Supporting R Scripts 35
Appendix C. Model Parameters 38

List of Acronyms 39

LIST OF FIGURES

Figure 1. Schematic of the Physiological Response to Hypoxia via the Carotid Body 3
Figure 2. pO2 Levels in Arterioles, Venules, and Tissue Sites in the Venous Capillary Network 5
Figure 3. Binding Sites on HIF-1α Protein 7
Figure 4. Hemoglobin and Oxygen Binding Curves 9
Figure 5. Schematic of the Oxygen Transport Model 10
Figure 6. Schematic of the HIF-1α Pathway in Cells Such as Neurons 12
Figure 7. Schematic Representation of the Kinetic Model 13
Figure 8: Simulated Kinetics of O2 in Arterial Blood, Brain Blood, and Brain Tissue 15
Figure 9. Simulated Kinetics of HIF-1α in Brain Cytosol and Nucleus, Together with Transcription Signal 16
Figure 10. Transcription Signal (TC) Fits to mRNA and VEGF Data 17
Figure 11. Schematic of a Simple Differential Equation Based Model of Gene Expression 18
Figure 12. HIF-1 α and Capillary Density in Hypoxic Rat Cerebral Cortex 19
Figure 13. Relation between Brain Tissue Hypoxia, Neuroinflammation and Performance Degradation 21
Figure 14. Changes of Plasma IL-6 Levels over Time 22
Figure 15. Schematic of a Potential Model for Oxygen Sensing in the Carotid Body 23

LIST OF TABLES

Table 1: Normal (Mean) Values of Oxygen Concentration in Healthy Humans 4
Table 2. Brief Summary of Some Existing Models of the HIF-1α Pathway 8

THIS PAGE INTENTIONALLY LEFT BLANK.

PREFACE

Funding for this project was provided through the Aerospace Toxicology Program, which is part of the Aerospace Physiology and Toxicology Program in the 711th Human Performance Wing of the Air Force Research Laboratory. This research was conducted under cooperative agreements FA8650-10-2-6062 and FA8650-15-2-6608, both with the Henry M. Jackson Foundation for the Advancement of Military Medicine (HJF). The program manager for the HJF cooperative agreements was David R. Mattie, PhD (711th HPW/RHDJ), who was also the technical manager for this project.

THIS PAGE INTENTIONALLY LEFT BLANK.

1.0 SUMMARY

Episodes of hypoxia-like events experienced by F-22 pilots after training missions have raised questions about pilot exposures and their effective mission accomplishment. These episodes identified data gaps in the understanding of pilot exposures in high performance aircraft. We, therefore, need to understand how diminished levels of oxygen at lower than atmospheric pressure may cause physiological hypoxia, and how temporary loss of this metabolic and physiologic requirement relates to alterations in cognition.

Responses to hypoxia take place at multiple levels within the human body. The initial response is through the carotid body altering physiology (breathing rate, regional blood flow). Tissue level responses involve regulating demand for oxygen through altered function. Key to understanding these responses both at the physiological and tissue (brain) level are oxygen sensing pathways, particularly those involving the oxygen sensing cytosolic gene transcription factor HIF-1α. These linked oxygen sensing pathways need to be understood mechanistically and quantitatively for defining response changes and assessing changes in cognition.

A mathematical model was developed to integrate these experimental measurements and provide a description of the mechanisms of hypoxia and the mammalian organism's response. Our model focuses on oxygen delivery to the brain. It includes delivery of oxygen to the blood via hemoglobin binding, breathing rate and cardiac output, delivery of oxygen from the blood to the brain tissue, and finally the response of the HIF-1α signaling pathway in terms of alterations in gene expression and other end-points. The model simulates time courses of tissue (brain) oxygen, intracellular HIF-1α, transport to the nucleus, binding to hypoxia responsive element (HRE) and generation of transcription signal, during altered blood oxygen levels. Model development is an iterative process; the model described here is sufficient to describe these underlying mechanisms, and provides a firm basis for further development, should the need arise to incorporate additional data. Several such potential data extensions that would advance the model are outlined.

The HIF-1α model is partially parameterized based on experimental data in the literature, as well as existing models related to or including the HIF-1α signaling pathway. The model has been fitted to (literature) steady-state dose/response data for vascular endothelial growth factor (VEGF) and VEGF mRNA. The model also describes angiogenesis data (longer term changes in capillary densities in response to prolonged hypoxia exposures), while assuming linearity of dose/response for gene transcription process.

In vitro cultured cell studies are useful for elucidating elements of these processes. These data need to be integrated and applied (extrapolated) to relevant human exposure scenarios in order to assess the relevance of hypoxia to the abovementioned Air Force (AF) issues. Mathematical models of the kind described here are essential both for the understanding of *in vitro* results investigating underlying mechanisms, and in order to extrapolate these results to *in vivo* and relevant human scenarios.

This report continues and concludes the work initiated in a previous Technical Report AFRL-RH-WP-TR- 2016-0086: *Host - HIF-1α Pathway and Hypoxia: In Vitro Studies and Mathematical Model*, by Robinson and others.

2.0 INTRODUCTION

2.1 Background

There are currently issues with multiple aircraft in the US armed forces, including the AF F-22, F-35, A-10 and Navy F/A-18, possibly related to hypoxia, as well as other conditions, such as hyperoxia and hypobaria, that may negatively impact pilot performance (Martin *et al.*, 2012). In addition, pilots of the high-altitude U-2 reconnaissance aircraft may suffer brain lesions (white matter hyperintensities) and cognitive deficits (McGuire *et al*., 2014). In light of these issues, we need to understand how oxygen delivery (as a result of both concentration and air pressure changes) relates to alterations in brain functioning. In addition to oxygen alone, we also need to understand the kinetics of potential contaminants under different oxygen conditions. Physiologically-based pharmacokinetic (PBPK) models have been developed in our lab for numerous chemicals and mixtures of concern. However, no PBPK models of combined oxygen and chemical contaminant exposure has been developed.

Organisms respond to low oxygen levels in the air in a number of ways. An initial response is through carotid body (CB) that mediates alterations of physiology (breathing, heart rate/blood flow). Tissue level responses involve regulating demand for oxygen through altered function. Key to understanding these responses both at the physiological and tissue (brain) level are oxygen sensing and response pathways, particularly those involving hypoxia inducible factor-1-alpha (HIF-1α). These linked pathways need to be understood mechanistically and quantitatively. *In vitro* studies are useful for elucidating elements of these processes. These approaches need to be integrated and applied (extrapolated) to relevant human exposure scenarios in order to assess the relevance of hypoxia to the abovementioned AF issues. Initial *in vitro* studies have been described in a previous Technical Report AFRL-RH-WP-TR-2016-0086: *Host - HIF-1α Pathway and Hypoxia: In Vitro Studies and Mathematical Model*, by Robinson *et al*.

Compensatory mechanisms for hypoxia in brain (and other tissues) work at a number of time scales, and include physiological and cellular responses. Physiological responses are fast-acting, and prevent cellular hypoxia (within limits). These responses are typically mediated by the carotid (and aortic) body, which is a sensory organ for detecting arterial blood O_2 levels and mediating systemic cardiac, vascular and respiratory responses to hypoxia. Carotid body (CB) response travels via afferent nerves that carry signals back from the carotid and aortic bodies to the brainstem, which responds accordingly by, for example, increasing the ventilation rate. Figure 1 illustrates this adaptive response to hypoxia.

Responsiveness of the CB to acute hypoxia relies on the inhibition of O_2-sensitive K^+ channels in glomus cells, which leads to cell depolarization, Ca^{2+} entry and release of transmitters that activate afferent nerve fibers; the molecular mechanisms underlying K^+ channel modulation by O_2 tension may involve disruption of the prolylhydroxylase/ hypoxia inducible factor pathway (Lopez-Barneo *et al.*, 2008). Evidence that HIF-1α is involved with carotid body responses to hypoxia includes studies with HIF-1α +/- mice (Kline *et al*. 2002; Peng *et al*. 2006), in which the hypoxia response was severely impaired. However, there is some disagreement, with some researchers thinking it unlikely that acute responses to hypoxia by the carotid body (such as

regulation of breathing and heart rate) are mediated directly by the HIF-1α pathway (Wyatt, personal comm.). In the case of chronic hyperoxia, the O_2-sensitive response is diminished (leading to cell hyperpolarization) while the hypercapnic (blood CO_2 retention) response is augmented (Sinski *et al*., 2014).

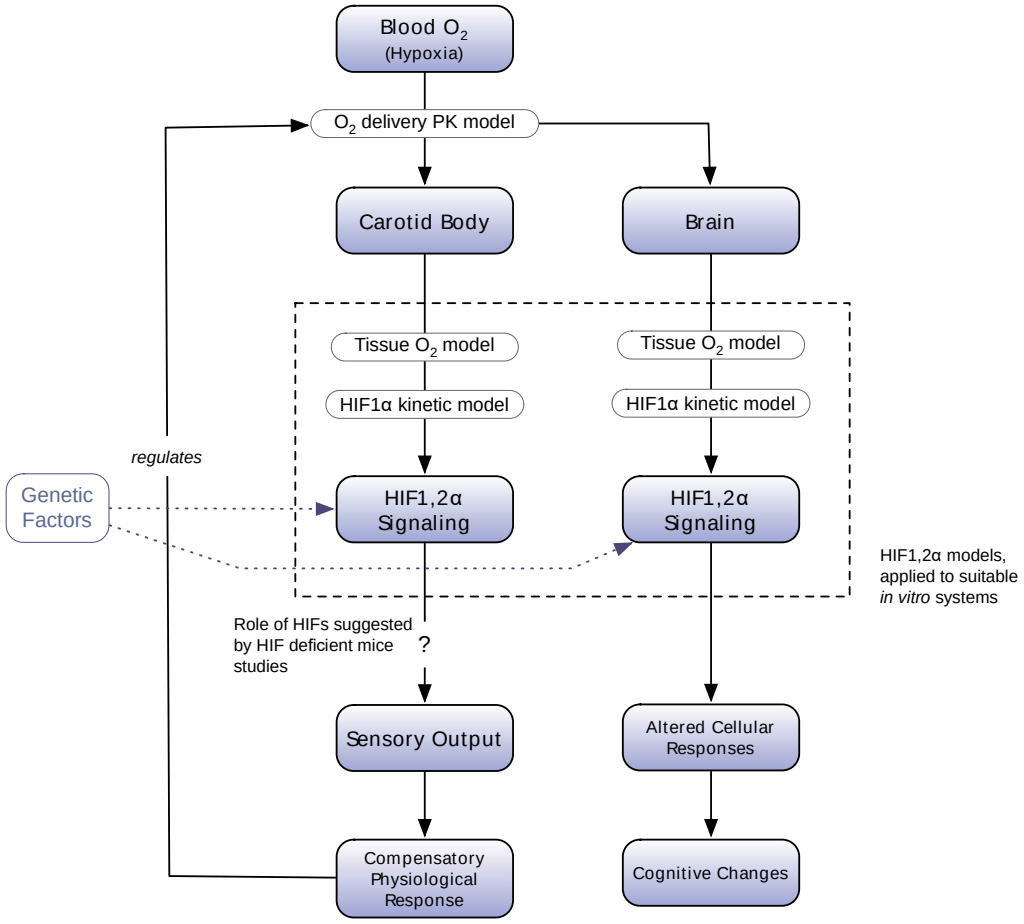

Figure 1. Schematic of the Physiological Response to Hypoxia via the Carotid Body. Figure also shows the tissue response to hypoxia, both mediated by the HIF-1α signaling pathway

When such first tier, physiological protection mechanisms are inadequate, cellular hypoxia ensues, and affected cells such as neurons adapt to the hypoxic conditions by altering homeostasis through gene-regulated cellular processes such as metabolism, apoptosis, angiogenesis and cell proliferation and differentiation.

We propose to develop a mechanism-based model for an organism's response to hypoxia. Our model involves two interlinked parts: Firstly, a whole body oxygen delivery model that determines blood oxygen levels from inhaled air; and secondly, a HIF-1α signaling model that determines the tissue response.

2.2 Oxygen Transport to Tissues

About 98.5 percent of the oxygen in the arterial blood in a healthy human at sea-level pressure is bound to hemoglobin, while the remaining 1.5 percent is dissolved in the plasma and other blood liquids. The hemoglobin molecule is the primary transporter of oxygen in mammals and many other species. Hemoglobin has an oxygen binding capacity of 1.368 ± 0.017 (mean ± standard deviation) mL O_2 per gram hemoglobin (Dijkhuizen *et al*., 1977). Table 1 shows Normal values of oxygen concentration in healthy humans, expressed in mmHg (partial pressure), percent O_2, and mmol/L.

Table 1: Normal (Mean) Values of Oxygen Concentration in Healthy Humans

Location	pO2 (mmHg)	%O2	mmol/L
Air	160	21.0	8.3
Trachea	150	19.7	7.8
Alveoli: 100-120 mmHg	110	14.4	5.7
Lung inflow (arterial): 80-100mmHg	90	11.8	4.7
Lung outflow (venous)	40	5.2	2.1
Arterial	100	13.1	5.2
Venous	40	5.2	2.1
Brain#	35	4.6	1.8

Notes: Adapted from Carreau *et al.* (2011); # Dings *et al*. (1998) measured brain oxygen concentrations as a function of depth using a brain inserted probe in human patients, and observed mean pO_2 of 23.8 ± 8.1 mmHg at 22 to 27 mm below the dura, 25.7 ± 8.3 mmHg at 17 to 22 mm, 33.0 ± 13.3 mmHg at 12 to 17 mm and 33.3 ± 13.3 mmHg at 7 to 12 mm. The "scientific community agrees to say that if the brain tissue pO_2 is above 35 mmHg (4.6 percent), normal oxygenation of the brain tissue should be assured" (Carreau *et al.*, 2011).

As an example of brain tissue and blood oxygen rapid responses to short periods of hypoxia, Figure 2 shows pO_2 levels in arterioles, venules, and tissue sites in the venous capillary network during a 1-minute control period, 1-minute reduction of inspired oxygen fraction from 21 percent to 7 percent, and 2-minute recovery period (Johnson *et al*., 2005).

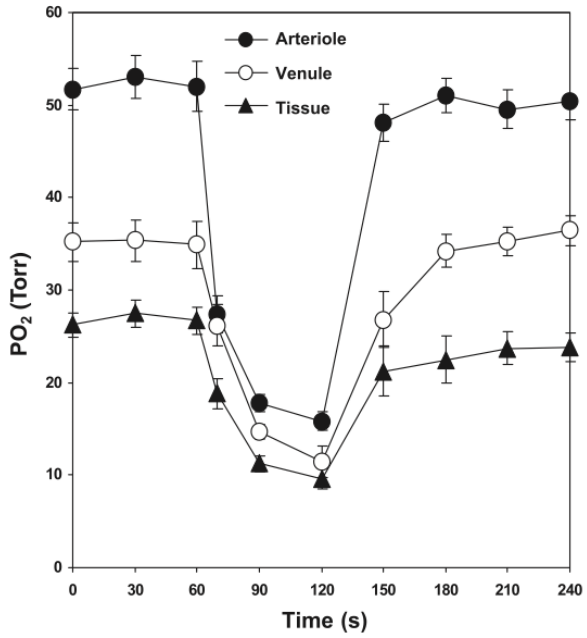

Figure 2. pO_2 Levels in Arterioles, Venules, and Tissue Sites in the Venous Capillary Network. Figure shows response during a 1-minute control period, 1-minute reduction of inspired oxygen fraction from 21 percent to 7 percent, and 2-minute recovery period at 0.21. Data points are means +/- SE. Data from Johnson *et al*. (2005).

The literature is rich with models of oxygen transport and cardiopulmonary control, at various levels of physiological detail (Grodins *et al.*, 1967; Duffin *et al.*, 2000; Topor *et al.*, 2004; Ward, 2007; Wolf and Garner, 2007; Benson *et al.*, 2013; Cheng *et al.*, 2016). For example, Topor *et al.* (2004) have developed a mathematical model that describes multiple mechanisms associated with control of breathing in response to hypoxia. Although these models are adequate for predicting oxygen transport, the model equations are in quite a different format than those of our typical PBPK models for chemical contaminants, making the combination of the models difficult. Therefore, a goal of this effort was to investigate the applicability of our PBPK approach to the transport of oxygen.

The impact of chemical contaminants on oxygen transport is often through an allosteric shift in oxygen-hemoglobin binding. For example, organic phosphates, such as 2,3-Diphosphoglycerate (2,3-DPG) binds to hemoglobin and rearranges it into a tense state, which decreases its affinity for oxygen. Carbon monoxide (CO) is also a classic example of a compound interfering with the oxygen transport function of the blood by combining with hemoglobin to form hemoglobin (COHb) (see, for example, Berne *et al.*, 2004). CO has approximately 200 times the affinity for hemoglobin that oxygen does and for that reason even small amounts of CO can tie up a large proportion of the hemoglobin in the blood making it unavailable for oxygen carriage. If this happens, the pO_2 of the blood and the hemoglobin concentration will be at normal levels, but the the oxygen concentration and transport to the tissues will be grossly reduced.

2.3 HIF-1α Pathway

In both the carotid bodies (Prabhakar, 2013), and other tissues, the primary sensing molecule is the hypoxia inducible factor (HIF-1α) transcription factor protein. The presence of oxygen activates prolyl hydroxylases (PHD) to hydroxylate HIF-1α, leading to HIF-1α protein degradation. Under low oxygen conditions, hydroxylase inactivity allows HIF-1α protein to accumulate, which in turn initiates target gene expression. HIF-1α dimerizes with HIF-1β and translocates to the nucleus where it associates with CBP (CREB binding protein) and DNA polymerase II and then binds DNA to initiate transcription, up-regulating expression of apoptotic cell death pathway genes, angiogenic genes, erythropoeitic genes and other protein genes.

Figure 3 shows the interactions of the HIF-1α protein under conditions of normoxia and hypoxia. Under normoxic conditions, hydroxylation of Pro-402 and Pro-564 by the HIF-1α prolyl hydroxylases (PHD) allows binding of von Hippel-Lindau tumor suppressor protein (VHL), which permits HIF-1α ubiquitination and degradation, maintaining low levels of HIF-1α in the cytosol. At the same time, hydroxylation of Asn-803 by FIH1 (factor inhibiting HIF-1) prevents the interaction of HIF-1α with the cofactors p300 and CBP (CREB binding protein). Under hypoxic conditions, hydroxylation is less likely, VHL does not bind and HIF-1α builds up in the cytosol. At the same time, binding of p300/CBP cofactors facilitates HIF-1α protein translocation to the nucleus and subsequent gene transcription (Semenza, 2004).

A number of experimental studies can be done to elucidate the mechanisms associated with both the physiological and cellular responses to hypoxia. *In vivo* studies can be used to explore the physiological responses mediated by the carotid body. In addition, there is the possibility of looking at HIF signaling in cultured Type 1 carotid bodies. In general, *in vitro* studies can be used to study hypoxia responses in specific cell types such as neurons. For example, high-throughput *in vitro* screening can be used to monitor expression of HIF-1α, determine proteomic profiles of hypoxic events and identify potential protein markers for further investigation from brain tissues collected from *in vivo* studies. Immunohistochemical staining (IHC) of whole brain from altitude studies was performed to identify regions most affected by hypoxia. A HIF-1α specific antibody can be used to see cytosolic and nuclear accumulation of HIF-1α. Protein biomarkers identified from *in vitro* studies can also be evaluated by IHC. Finally, it is also possible to measure mRNA levels of relevant proteins in the hypoxia signaling pathways.

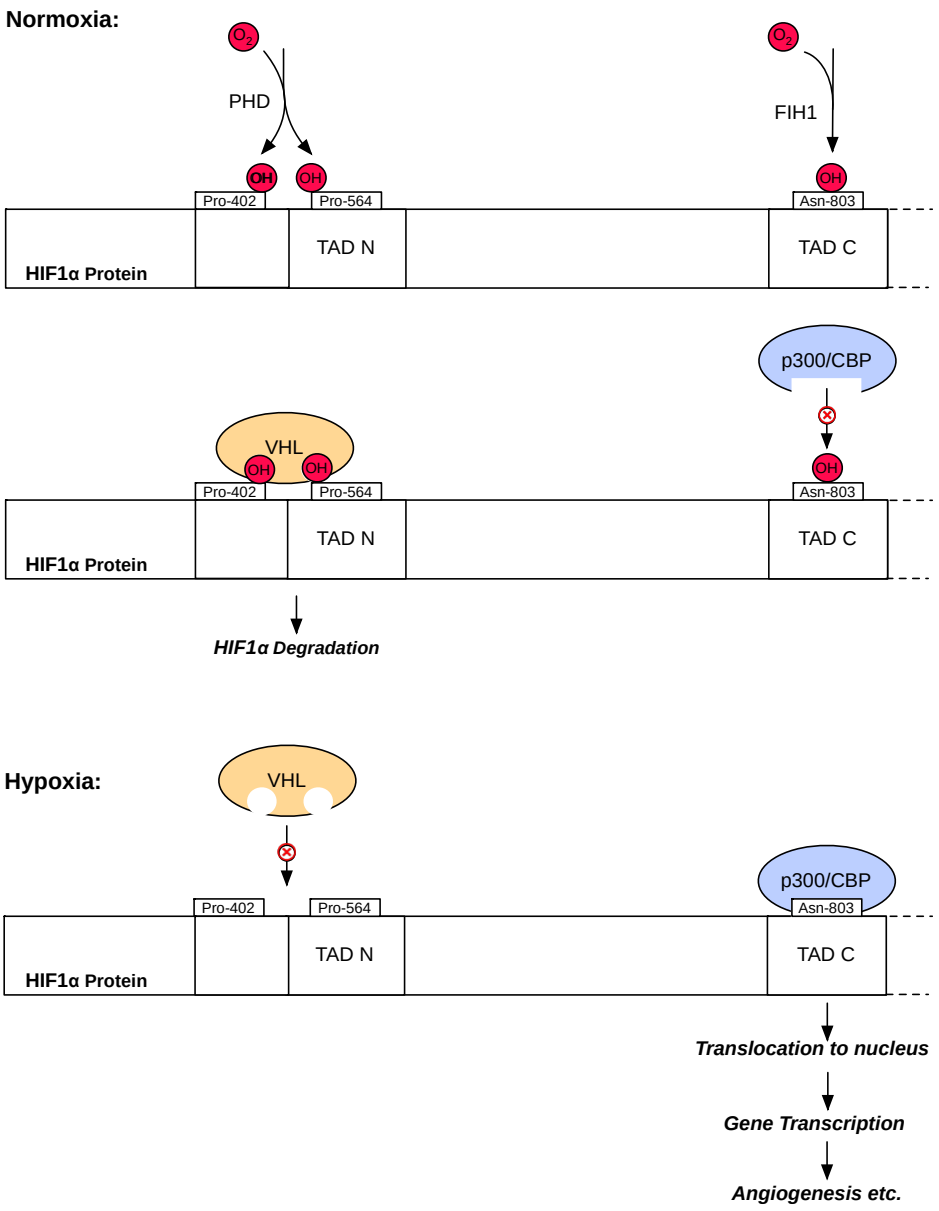

Figure 3. Binding Sites on HIF-1α Protein. N- and C-terminal transactivation domains (TAD N and TAD C) are regions for HIF-1α degradation and transcriptional activation, respectively. Under normoxic conditions, hydroxylation of Pro-402 and Pro-564 by the HIF-1α prolyl hydroxylases (PHD) allows the von Hippel-Lindau tumor suppressor protein (VHL) to bind, which permits HIF-1α ubiquitination and degradation, maintaining low levels of HIF-1α in the cytosol. At the same time, hydroxylation of Asn-803 by FIH1 (factor inhibiting HIF-1) prevents the interaction of HIF-1α with the cofactors p300 and CBP (CREB binding protein). Under hypoxic conditions, hydroxylation is less likely, VHL does not bind and HIF-1α builds up in the cytosol. Also, binding of p300/CBP cofactors facilitates translocation to the nucleus and subsequent gene transcription. (Adapted from Semenza, 2004).

2.4 Summary of Existing Mathematical Models

Table 2 shows a summary of some existing models for the HIF-1α pathway. At this point, our current model does not include hydroxylation of Asn-803 by FIH1 (factor inhibiting HIF-1), which prevents the interaction of HIF-1α with the cofactors p300 and CBP (CREB binding protein). Under hypoxic conditions, hydroxylation is less likely, VHL does not bind and HIF-1α builds up in the cytosol. At the same time, binding of p300/CBP cofactors facilitates translocation to the nucleus and subsequent gene transcription (Semenza, 2004) – see Figure 3. A number of models do include this process (see Table 2). However, the model described in the current Report is sufficient to describe the build-up of cytosolic HIF-1α under hypoxic conditions, and provides a firm basis for further model development, should the need arise to incorporate or describe additional data (or as such data become available).

Table 2. Brief Summary of Some Existing Models of the HIF-1α Pathway

Model Reference	Model Description	Notes
Kohn et al., 2004	HRE occupancy and/or mRNA expression in response to changes in oxygen concentration.	Initiated mathematical modelling of the HIF pathway.
Kooner et al., 2006	HRE occupancy and/or mRNA expression in response to changes in oxygen concentration.	Extended Kohn's model with role of oxygen in mediating reactions, as well as its transfer to nucleus.
Yu et al., 2007	HRE occupancy and/or mRNA expression in response to changes in oxygen concentration.	Uses "extreme pathway analysis" rather than solving system of ODEs
Qutub & Popel 2006	Sensitivity of HIF protein to hydroxylation cofactors and PHD	
Qutub & Popel 2007	Temporal effect on HIF protein stabilisation by succinate inhibition and PHD negative feedback.	
Yucel & Kumaz 2007	Sensitivity of the angiogenic behaviour of a cancer cell to PHD and FIH.	
Dayan et al., 2009	FIH controls a switch between C-TAD and N-TAD HIF target gene repertoires	
Schmierer et al., 2010	Sequestration of FIH modulates FIH activity	
Nguyen et al., 2013	Global temporal dynamics of the HIF:PHD:FIH network.	Estimation of some parameters to in-house experimental data

Adapted from Cavadas *et al*., 2013

3.0 METHODS

3.1 Oxygen Delivery Model

Table 1 above shows the decrease in oxygen concentration in the air as it passes from the external environment, down the trachea into the alveolar region. This decrease is primarily due to the increase in water vapor concentration in the air as it becomes progressively more humidified. Oxygen in the lung alveolus then partitions into the blood and binds to hemoglobin. Figure 4

shows the saturation curve for hemoglobin (A), together with the (computed) relationship between free and bound oxygen at equilibrium (B). In (A), the solid line shows the degree of hemoglobin saturation (left y-axis) and the concentration of the bound component in the blood (right y-axis), as a function of pO_2. The broken lines (with the right-hand axis) show the contribution of the unbound (free, dissolved) component both as it contributes to the total (upper curve) and its absolute concentration (lower curve).

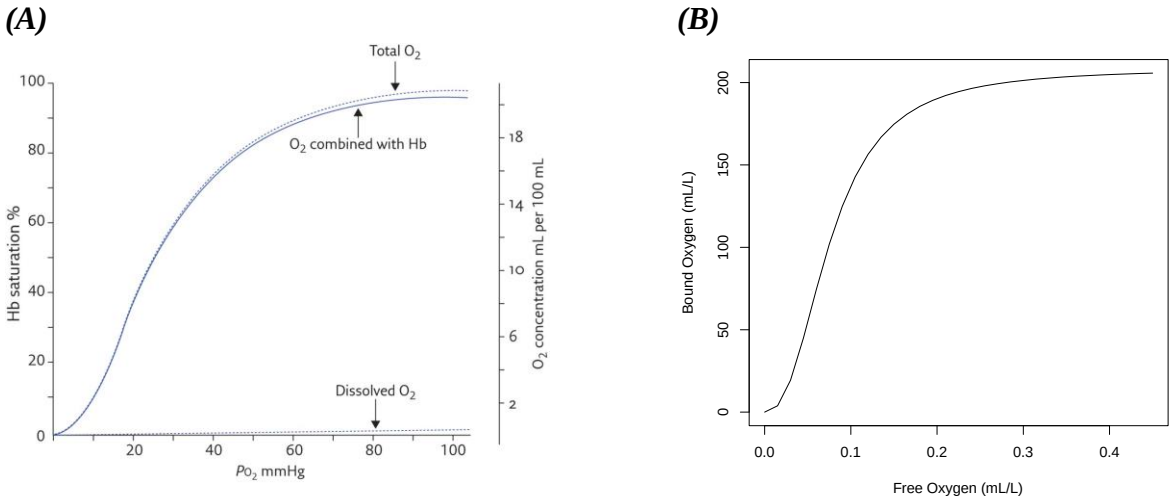

Figure 4. Hemoglobin and Oxygen Binding Curves. (A) The solid line shows the degree of hemoglobin saturation (left axis) and the concentration of the bound component in the blood (right axis) as a function of pO_2. The broken lines (with the RH axis) show the contribution of the unbound (free, dissolved) component both as it contributes to the total (upper curve) and its absolute concentration (lower curve) (adapted from Collins *et al*., 2015). (B) Relationship between bound (y-axis) and free (x-axis) oxygen concentrations.

Figure 5 shows a schematic of the oxygen transport portion of our model. Oxygen enters the alveolus in air saturated with water vapor at a partial pressure of 47 mmHg, at a ventilation rate of Q_P. Oxygen diffuses into the blood with a relative affinity or partition coefficient of *PB*. We assume that oxygen in the blood rapidly binds to hemoglobin, so that free (C_F) and bound (C_B) oxygen in the blood are in instantaneous equilibrium. The oxygenated arterial blood ($C_A = C_F + C_B$) is carried from the lungs to the rest of the body by the cardiac output blood flow (Q_c). Once the oxygenated blood reaches the brain, the higher pH in that tissue (due to local carbon dioxide accumulation from metabolism) facilitates the release of bound oxygen for diffusion into the tissue. In our model we assume that both bound and free oxygen are equally available for uptake, which is limited by an effective permeability-surface area product (*PA)* and a brain partition coefficient (*PBr*). Oxygen's dissociation from hemoglobin is heavily influenced by the tissue pH, therefore the brain's pH is incorporated into *PBr*. Inside the tissues, oxygen is removed via a saturable metabolic rate (*VMax, KM*). The blood from the brain and rest of the body is combined in a mixed venous blood compartment (concentration C_V) and returned to the alveolar region. The model was implemented in R (R Core Team, 2016), and the code is shown in Appendix A. Supporting R scripts are shown in Appendix B.

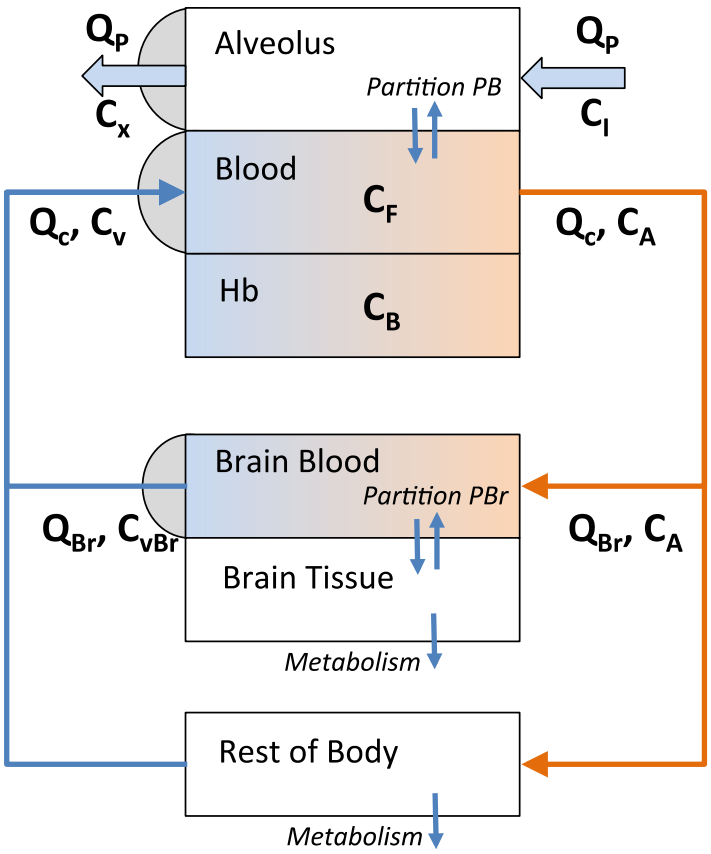

Figure 5. Schematic of the Oxygen Transport Model. Oxygen in the lung alveolus diffuses into the blood, binds to hemoglobin, and is transported to the tissues where it is metabolized (converted to CO_2).

Oxygen binding to hemoglobin is described using a Hill equation relating free oxygen dissolved in plasma to bound oxygen:

$$C_B = \frac{Bmax * {C_F}^n}{KD^n + {C_F}^n} \qquad \text{(Equation 1)}$$

The parameters, *Bmax*, *KD*, and *n*, are determined with the help of the equation for the total oxygen content of the blood:

$$C = 1.39 * Hgb * SaO_2 + 0.03 * PaO_2 \qquad \text{(Equation 2)}$$

The first term gives the amount of oxygen bound to hemoglobin (C_B), where *Hgb* is the amount of hemoglobin (*g/L*), SaO_2 is the fraction saturation of Hgb, and 1.39 is the amount of oxygen per gram of Hgb. The second term is the amount dissolved (C_F), where 0.03 is the solubility of oxygen in the blood, and PaO_2 is the partial pressure of oxygen in the blood. [Note that SaO_2 is a function of PaO_2, which is in fact the oxygen dissociation curve.]

A series of PaO_2 were generated and used in turn to generate a series of corresponding C_B and C_F values, using typical values for a healthy adult for *Hgb*, SaO_2, and PaO_2. The values were then used to obtain parameters fits for the above Hill equation using the "nls()" function, a nonlinear regression function in the software R.

Now what remains is to describe how C_F was determined. The rate equation for the arterial blood is the following:

$$\frac{dA}{dt} = Q_P * (C_I - C_F/PB) + Q_C * (C_V - C_A) \quad \text{(Equation 3)}$$

where Q_P is the pulmonary blood flow rate, C_I is the inspiratory alveolar oxygen concentration, C_F/PB (C_X) is the exhaled oxygen concentration, Q_C is the cardiac blood output, C_V is the mixed venous blood concentration, and $C_A = C_F + C_B$ is the total arterial blood concentration. We assume that equilibration of oxygen between the alveoli and blood is rapid, and thus set the derivative equal to zero, arriving at an equation that is solved implicitly for C_F at each step of the integration. With C_F computed, C_B can be calculated, and finally the C_A leaving the gas exchange region.

3.2 HIF-1α Mathematical Model for Brain

A mathematical model was developed to integrate these experimental measurements and provide a description of the mechanisms of hypoxia and the mammalian (or human) organism's response. The initial iteration of our model focuses on the brain. It includes delivery of oxygen to the cell, and the response of the HIF-1a signaling pathway in terms of alterations in gene expression (see Figure 6).

Our model is necessarily simplified. Our aim is to capture the essential behavior of the system in a way that relates to the available and relevant experimental data. Our initial model is partially parameterized, and initial estimates are made from parameter values in order to elicit appropriate model behavior. As experimental data is incorporated into the model, these parameter values will be updated and refined in an iterative manner. Briefly, the model assumes that oxygen movement from the blood into the intracellular space is determined by a permeability-surface area (*PA*) product. Once in the cell, it is removed via respiration at a maximum (saturable) rate V_{resp}. PHD hydroxylates HIF-1α, with intracellular levels of O_2 as a co-substrate (Semenza *et al*., 2004).

HIF-1α levels are determined from a balance of a constant zero order synthesis rate K_{HIF}, and a PHD-dependent degradation rate K_{PHD}. In addition, HIF-1α is transported into the nucleus, where it impacts gene expression. We assume a maximum transport rate T_{max}, and a half-saturation concentration of K_T.

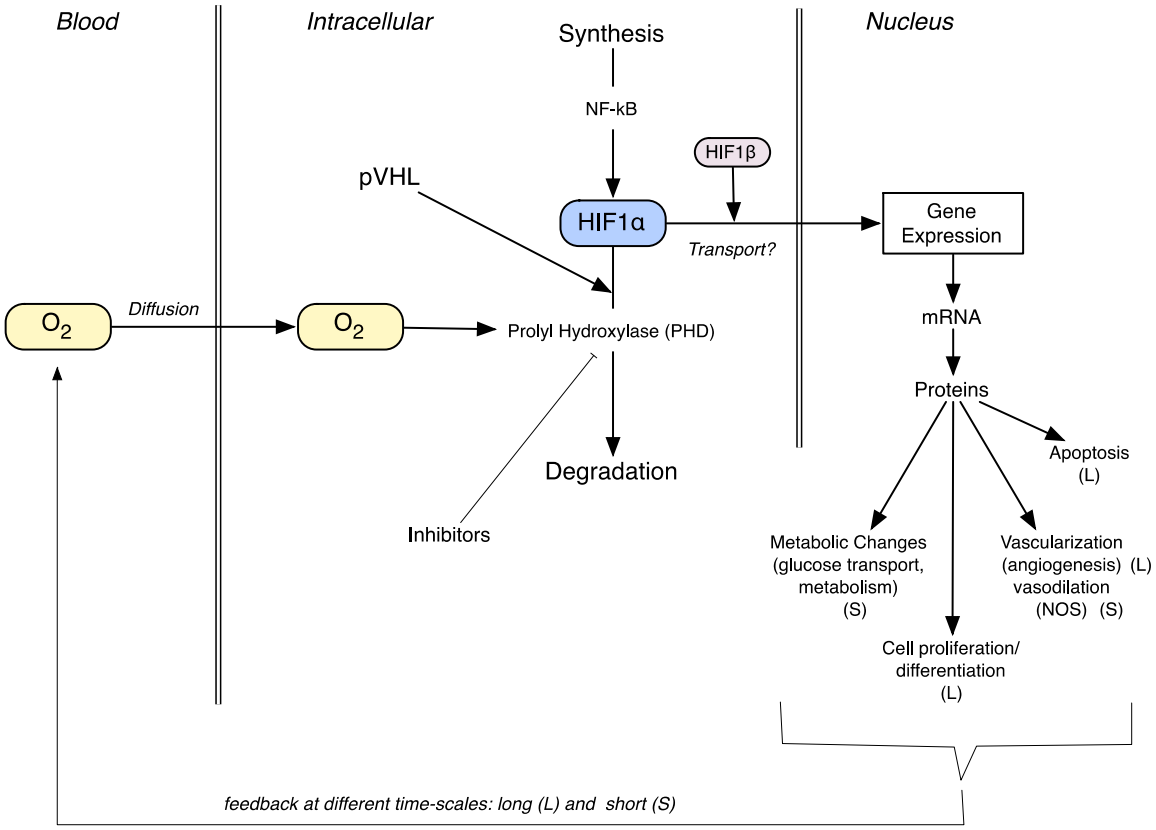

Figure 6. Schematic of the HIF-1α Pathway in Cells Such as Neurons. The pathway responds to cellular hypoxia by altering gene expression.

The equations describing O_2 and HIF-1α levels in the intracellular compartment (volume V_c) and the nucleus (volume V_n) are thus:

$$V_c \frac{d[O_2]_c}{dt} = PA.\left([O_2]_p - [O_2]_c\right) - \frac{V_{resp}.[O_2]_c}{K_{resp}+[O_2]_c} - K_{PHD}.[PHD].\frac{V_c.[HIF].[O_2]_c}{([HIF]+K_{mHIF})(K_{mO_2}+[O_2]_c)}$$

(Equation 4)

$$\frac{d[HIF]}{dt} = K_{HIF} - K_{PHD}.[PHD].\frac{[HIF].[O_2]_c}{([HIF]+K_{mHIF})(K_{mO_2}+[O_2]_c)} - \frac{T_{max}[HIF]}{[HIF]+K_T} \quad \text{(Equation 5)}$$

$$\frac{d[HIF]_n}{dt} = \frac{T_{max}[HIF]}{[HIF]+K_T} - K_{deg}^n[HIF]_n - K_{bm}[HIF]_n[HRE]\ , \quad \text{(Equation 6)}$$

where $[O_2]_p$ and $[O_2]_c$ are the concentrations (partial pressures) of oxygen in the plasma and cell intracellular compartments, $[PHD]$ and $[HIF]$ are the intracellular concentrations of prolyl hydroxylase and HIF-1α, respectively, and $[HIF]_n$ is the concentration of HIF-ndeg1α in the nucleus. Figure 7 shows a schematic of the model, with the modeled components in blue, and parameters or fixed values in red.

Once in the nucleus, HIF-1α is assumed to bind with hypoxia responsive element (HRE) on the DNA with a bimolecular rate constant K_{bm}, and is degraded according to a first order rate constant K^n_{deg} (equation 4). The binding of HIF-1α to HRE initiates a transcription signal TC, which is assumed to mediate gene transcription. TC is assumed to spontaneously decay at a rate K_{tc}:

$$\frac{dTC}{dt} = K_{bm}[HIF]_n[HRE] - K_{tc}.TC. \qquad \text{(Equation 7)}$$

These equations were incorporated into Berkeley Madonna (see Robinson *et al*., 2016) and also translated into "R", and combined with the oxygen transport model (Section 3.1 above) for the simulations that follow - see Appendix A and B.

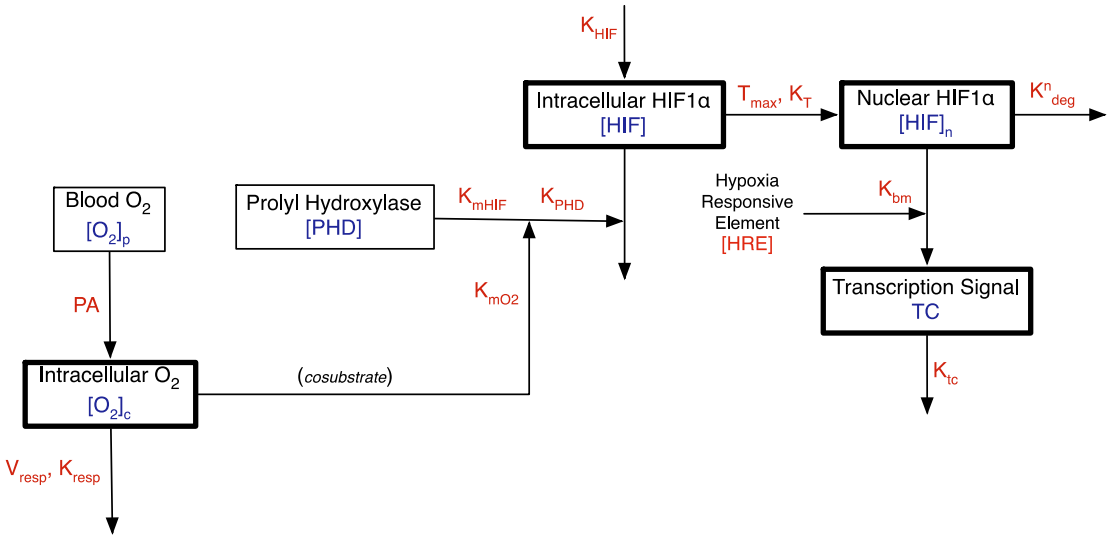

Figure 7. Schematic Representation of the Kinetic Model. Components whose concentration time course is modeled in response to changes in blood oxygen levels are shown in blue, while parameters or fixed values, that ultimately need to be experimentally determined, or fitted, are in red.

3.3 Parameter Values

A number of parameters for the model were gleaned from the published literature. K_{mHIF}, the Michaelis-Menten constant for HIF-1α as a substrate of PHD is reported as 100 nM (Hirsila *et al*., 2003; Koivunen *et al*., 2007; Kaelin and Ratcliffe, 2008, as reported by Nguyen *et al*., 2013). K_{PHD}, the catalytic rate constant for PHD-mediated hydroxylation of HIF-1α was taken to be 0.045 nM-1 s-1 (from Nguyen *et al*., 2013). K_{mO2}, the Michaelis-Menten constant for O_2 as a substrate of PHD is 250 µM (Hirsila *et al*., 2003; Koivunen *et al*., 2007; Kaelin and Ratcliffe, 2008, reported by Nguyen *et al*., 2013). A typical neuron has a volume of 10^5 um^2 (diameters range from 4 – 100 um in diameter – Davies, 2002), while the volume of nucleus is assumed to

be 5-25 percent of volume of neuron (we assume an average of about 15 percent). The basal HIF-1α synthesis rate used was 0.005 nM s^{-1} (Nguyen *et al*., 2013).

3.4 Integrating the Oxygen Transport and HIF-1 α Models

The oxygen transport and HIF-1 α models were combined by embedding the HIF-1 α model in the brain tissue compartment of the oxygen delivery model. (A number of parameters appear in both models, sometimes with different names; see *Appendix C: Model Parameters* for disambiguation). The rate equations for the brain tissue and cytoplasmic HIF-1 α were modified as follows to integrate the two. The equation for cellular oxygen in the HIF-1α model (equation 4) was modified to be consistent with the parameters in the oxygen delivery model, to yield:

$$\frac{dA_{Br,T}}{dt} = PA.\left(CV_{Br} - C_{Br,T}/P_{Br}\right) - \frac{VMax_{Br}.C_{Br,T}}{K_M + C_{Br,T}} - F.\frac{K_{PHD}[PHD][HIF].C_{Br,T}}{([HIF]+K_{mHIF})(C_{Br,T}+K_{mO_2})} \quad ,$$

(Equation 8)

where *A* is amount (mg) of oxygen, *C* is concentration (mg/L), and the subscript *Br* indicates brain, and *T* is for the brain *tissue* subcompartment. *F* is a conversion factor from nM/second to mg/hour, making use of the volume of the brain tissue. The HIF-1 α rate equation was modified by replacing $[O_2]_c$ with $C_{Br,T}$. The remaining HIF-1 α model equations (6 and 7) were added unchanged to the transport model.

4.0 RESULTS

4.1 Time-Course Simulations

The simulation of oxygen transport, HIF-1α kinetics, and transcription factor production using the combined model is shown in Figures 8 and 9. The scenario simulated is normoxia, or 21 percent oxygen inhaled for 6 hours, hypoxia, or 7 percent oxygen inhaled for 4 hours, and finally a return to normoxia. The model predicts a decrease in brain oxygen levels, a corresponding increase in HIF, and a resulting increase in transcription factor.

Simulations such as these can be used to describe and interpret experimental data in terms of underlying mechanisms. Such experiments, if quantitative, can also be used to calibrate and further parameterize the model.

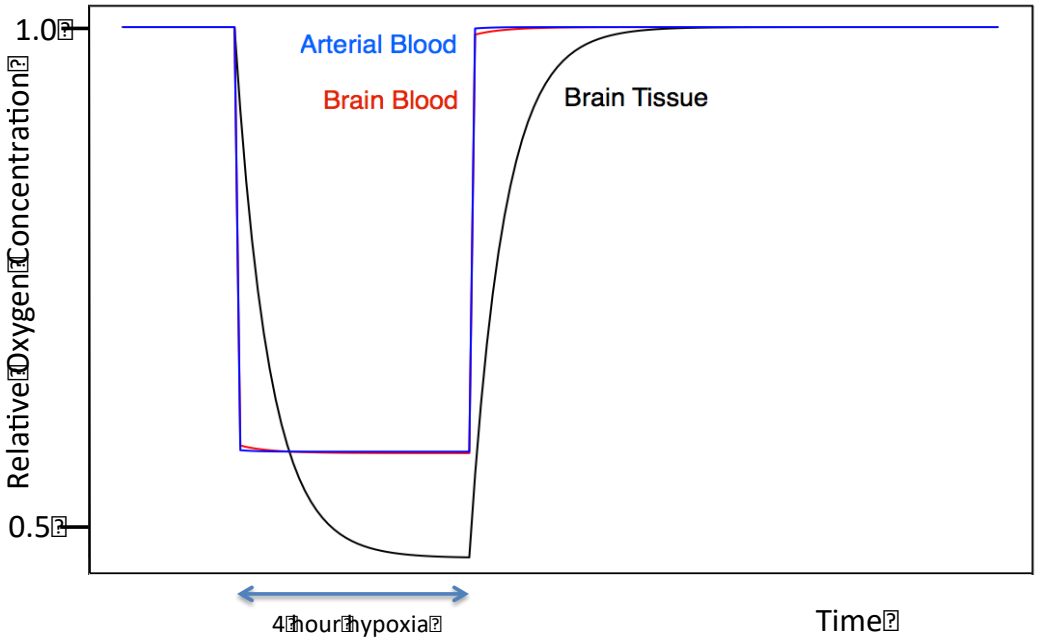

Figure 8: Simulated Kinetics of O_2 in Arterial Blood, Brain Blood, and Brain Tissue. Normoxia (21 percent), hypoxia (7 percent), and return to normoxia. Oxygen concentrations are normalized to levels under normoxia (1.0 for 21 percent O_2 in inhaled air), assuming a decrease in hemoglobin binding (and arterial concentration) at 7 percent O_2 by about 37 percent (see Figure 4A).

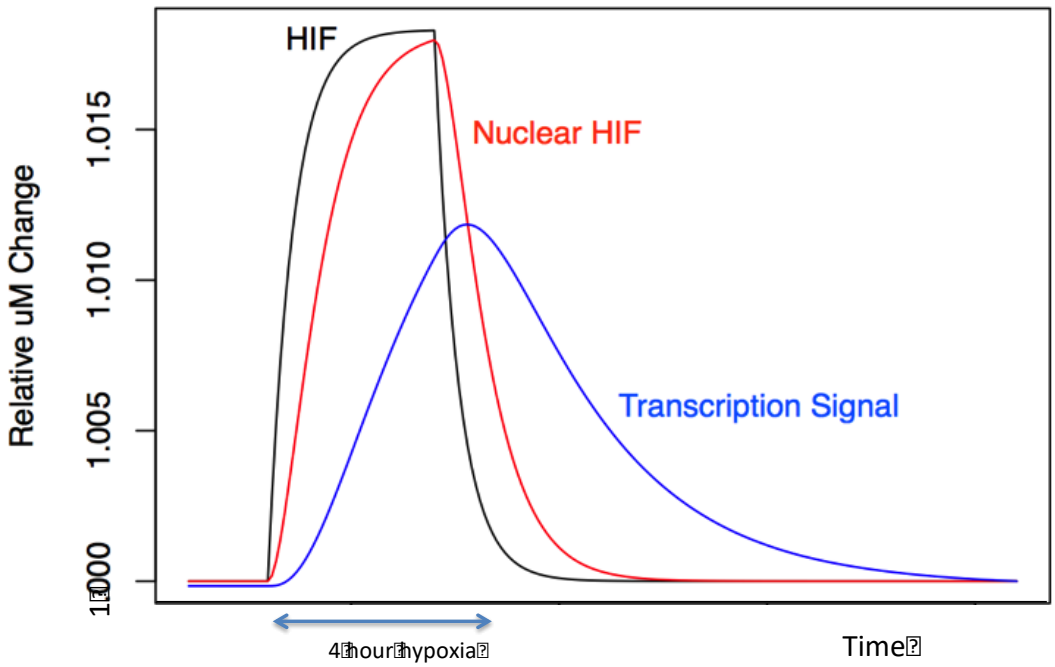

Figure 9. Simulated Kinetics of HIF-1α in Brain Cytosol and Nucleus, Together with Transcription Signal. Normoxia (21 percent), hypoxia (7 percent), and return to normoxia.

4.2 Dose-Response Simulations

Although the model can be extended to include gene transcription (see Section 5.1 below), we can analyze steady-state (SS) gene transcription products without a detailed time-course model. For example, Schoch *et al*. (2002) measured the amount of VEGF protein and mRNA in the brain of mice following normobaric hypoxia at 12 percent - 6 percent oxygen for 24 hours *in vivo* using an ELISA (enzyme-linked immunosorbent assay) specific for murine VEGF and northern blots, respectively. These data are shown as the red and blue plots in Figure 10.

The mRNA and protein levels in the SS will be given by the ratio of their production and degradation rates. It is reasonable to assume that degradation rates are relatively constant, and in particular are not dependent on the degree of hypoxia or hyperoxia. Production rates, however, may reasonably be assumed to be proportional to the degree of hypoxia (linear dose/response), at least within reasonable limits. The SS levels of mRNA and protein will thus also be proportional to the (hypoxic) dose. If we further assume that in the SS, levels of protein and mRNA are proportional to the transcription signal given from our model TC (double the transcription signal leads to doubling of the SS levels of protein and message), we may fit the Schoch *et al*. (2002) dose/response data as shown in Figure 8, where we have plotted the ratio of protein and message at 12 percent, 10 percent 8 percent and 6 percent O_2, relative to normoxia (20 percent O_2), against the respective O_2 concentrations. Our results indicate that our model is able to reasonably fit the changing ratios of both VEGF protein and mRNA as a function of hypoxia, although the fitted value of prolyl hydroxylase enzyme activity (PHD) was lower by a factor of about 1.7/4 ~ 0.4 for the mRNA fit (Figure 10).

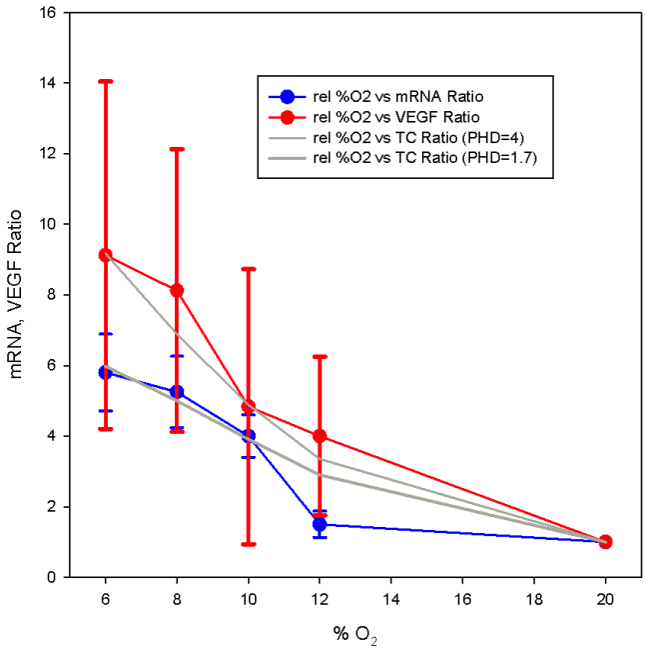

Figure 10. Transcription Signal (TC) Fits to mRNA and VEGF Data. The Y axis shows the ratio of protein and message at 12 percent, 10 percent 8 percent and 6 percent O_2, relative to normoxia (20 percent O_2), against the respective O_2 concentrations. Red curve represents measured VEGF protein levels, blue curve mRNA levels for VEGF. Gray lines represent model predictions, for different values of prolyl hydroxylase activity (PHD) optimized to fit each data set. Error bars represent standard deviations for the ratios. Data from Schoch *et al.* (2002).

5.0 CONCLUSIONS AND FUTURE WORK

5.1 Gene Transcription and Longer Term Effects

The model can be extended to include a gene transcription signal and gene transcription itself as output from the HIF-1α pathway. In such an extended model, the output from the current model (HIF-1α binding to the HRE and the resulting transcription signal) would provide an input to a model of gene expression, such as one provided by Chen *et al*., 1999 or Ay and Arnosti, 2011 (see Figure 11), thereby linking to angiogenesis and finally to alterations in capillary density (LaManna *et al.*, 2004).

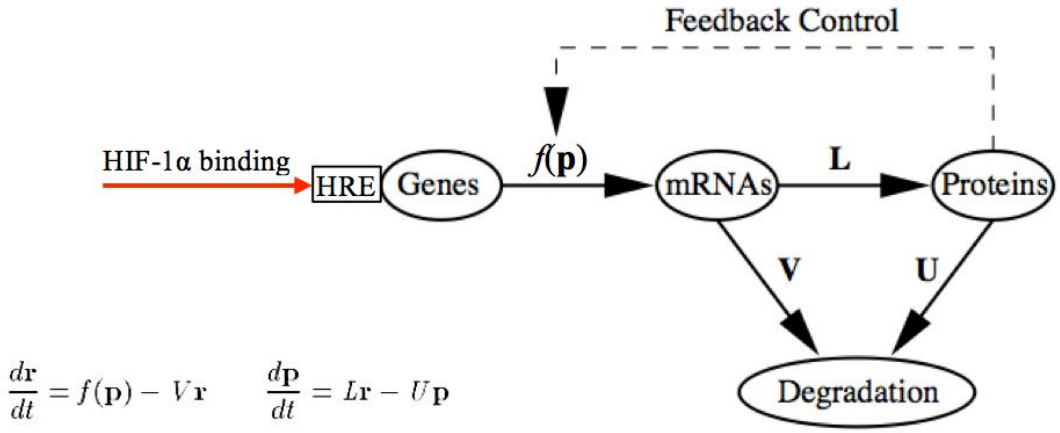

n	The number of genes in the genome;
$\mathbf{r}$	mRNA concentrations, n-dimensional vector-valued functions of t;
$\mathbf{p}$	Protein concentrations, n-dimensional vector-valued functions of t;
$f(\mathbf{p})$	Transcription functions, n-dimensional vector polynomials on $\mathbf{p}$;
L	Translational constants, $n \times n$ non-degenerate diagonal matrix;
V	Degradation rates of mRNAs; $n \times n$ non-degenerate diagonal matrix;
U	Degradation rates of Proteins, $n \times n$ non-degenerate diagonal matrix;
HRE	Hypoxia Responsive Element

Figure 11. Schematic of a Simple Differential Equation Based Model of Gene Expression. Based on Chen *et al*. (1999).

5.2 Capillary Densities and Angiogenesis

VEGF and other proteins, released from cells as a result of local hypoxic conditions, stimulate chemotaxis and proliferation in endothelial cells during capillary sprouting. Experimental data are available that explore the time-course of angiogenesis and changes in capillary density following extended periods of hypoxia, and return to normoxia. Figure 12 (A) shows HIF-1α measured in the cortex of rats exposed to hypoxic conditions for 6 hours to 21 days, relative to normoxic controls (0.5 atmospheres, equivalent to 10 percent normobaric oxygen) (Chavez *et al*., 2000). Figure 12 (B) shows capillary density in the rat cerebral cortex increased by 60 percent after 3 weeks of hypoxia (0.5 atmospheres, equivalent to 10 percent normobaric oxygen) and that it progressively decreased to prehypoxic values after 3 weeks of normoxic recovery (Pichiule and La Manna 2002). The latter is likely due to apoptosis of cells associated with excess capillary density that is no longer required under normoxic conditions. Both capillary density increases (due to angiogenesis) and decreases (due to apoptosis) have similar time scales, taking days or weeks to adjust, making them unlikely candidates to mediate more rapid changes in hypoxia or periods of rapid intermittent hypoxia.

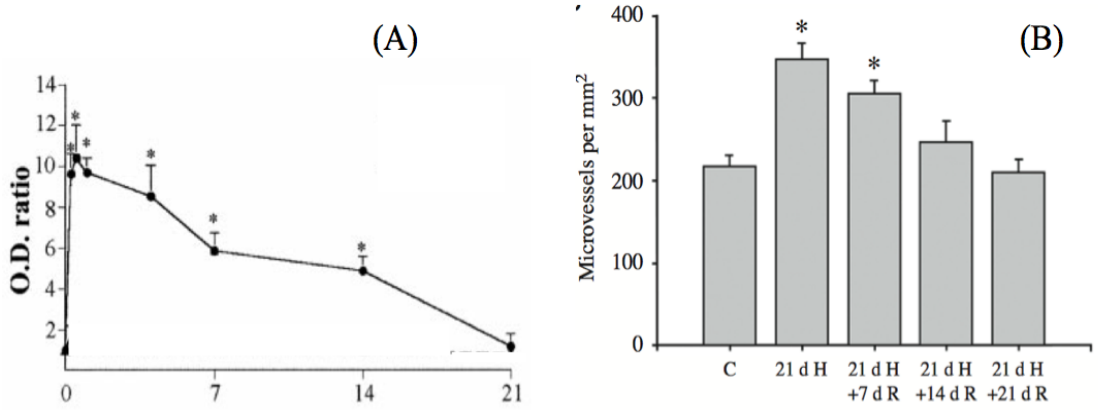

Figure 12. HIF-1 α and Capillary Density in Hypoxic Rat Cerebral Cortex. (A) HIF-1α Measured in the Cortex of Rats Exposed to Hypoxic Conditions: Exposure is for 6 hours to 21 days, relative to normoxic controls (0.5 atmospheres, equivalent to 10 percent normobaric oxygen) (Chavez *et al*., 2000). (B) Capillary Density in the Rat Cerebral Cortex: This increased by 60 percent after 3 weeks of hypoxia (0.5 atmospheres, equivalent to 10 percent normobaric oxygen) and that it progressively decreased to prehypoxic values after 3 weeks of normoxic recovery (adapted from Pichiule and La Manna 2002, based on photomicrographs of GLUT-1-stained sections).

Models of angiogenesis have been developed (see Qutub *et al*., 2009 for an overview). Basically, the process is as follows (Qutub *et al*., 2009):

1) HIF-1α is upregulated in a hypoxic cell. HIF-1α activates the transcription of VEGF, which is then secreted by the cell.
2) VEGF - VEGF-receptor binding on the capillary surface.
3) Vessel permeability changes.
4) An activated endothelial cell (the tip cell) starts to break down the basement membrane.
5) Stalk cells proliferate behind the tip cell.
6) The leading edge of the moving sprout releases matrix metalloproteinases, which proteolyze the surrounding extracellular matrix, allowing the cell to migrate.

Such a processes is necessarily multi-scale in nature – and multiscale modeling is an essential tool to truly understand a process of such biological complexity.

5.3. Inflammation

HIF can have both pro- and anti-inflammatory effects, and cross-talk between HIF and inflammatory pathways may be critical for understanding white matter hyperintensities (WMH) in U-2 pilots, since the latter are likely associated with neuroinflammation (Cavadas *et al.*, 2013; McGuire *et al*., 2013). VEGF induces angiogenesis, increased vascular permeability, and inflammation. VEGF has been shown to induce angiogenesis when infused continuously into adult rat brain tissue; in addition, VEGF has been shown to enhance permeability in brain vasculature (Vezzani, 2005).

Pilots of the high-altitude U-2 reconnaissance aircraft undergo repeated exposure to hypobaric conditions, and as a result may suffer brain lesions (white matter hyperintensities) and cognitive deficits (McGuire *et al*., 2014). All of the WMH observed in pilots were regionally uniformly distributed and located in deep white matter rather than in the cerebral cortex (McGuire *et al*., 2013), while there is a significant regional heterogeneity in the distribution of subcortical WMH in normal aging. The majority (60 percent–80 percent) of WMH are found in the frontal area, presumably because its high metabolic demand makes it more vulnerable to age-related cerebrovascular disorders. A more uniform distribution of WMH is a hallmark finding in many neuroinflammatory disorders and traumatic brain injury and may be used to gauge disease severity and progression, suggesting that hypobaric exposure produces white matter damage different from that occurring in normal aging. Other groups with increased WMH burden include high-altitude mountain climbers, in which WMH's are attributed to a combination of hypoxia and hypobaria (McGuire *et al*., 2013), and high altitude chamber operators (McGuire *et al*., 2014b). The latter study provides strong evidence that non-hypoxic hypobaric exposure may induce subcortical WMHs in a young, healthy population lacking other risk factors for WMHs (McGuire *et al*., 2014b).

The circulation of U-2 pilots (and high altitude chamber operators) is purged of nitrogen (degassed) prior to each mission with 100 percent oxygen for 1 hour (McGuire *et al*., 2014). This may not, however be sufficient, since gases readily diffuse across the mucosa. The direction of diffusion is dictated by the partial pressure of that gas in blood versus luminal contents. For methane and hydrogen, diffusion is always out of the lumen into blood. Nitrogen and CO_2 diffuse in either direction, depending on specific conditions within the individual. We thus postulate that microinfarcts can be produced by nitrogen bubbles, inducing microvascular occlusions (McGuire *et al*., 2013). Damage produced by interaction between microemboli and cerebral tissue, may lead to thrombosis, coagulation, inflammation, and/or activation of innate immune response. Injury may thus be produced by microemboli entering cerebral circulation at random.

According to McGuire *et al*., (2013), three potential sources of microemboli should be considered: microbubbles of gas, presumably nitrogen; platelet-based thrombi; and microparticles.

- Microbubbles: symptoms of decompression sickness classically are believed secondary to nitrogen gas bubbles exerting direct pressure on tissues, blocking small arteriolar vessels, and interacting with blood proteins
- Microthrombi: occlusion of small cerebral vessels by platelet thrombi produced by accelerated coagulation of blood in the presence of venous nitrogen gas bubbles
- Platelet aggregation.

Thus, vascular damage or tissue damage caused by these processes induces (and is exacerbated by) an inflammatory response. In addition, IL-1β (and potentially other cytokines) released by microglia and macrophages impacts long term potentiation (LTP) and memory formation (Lynch, 2010), potentially leading to the observed cognitive issues in U-2 pilots (McGuire *et al*., 2014) (see Figure 13).

Furthermore, and more generally, periods of hypoxia, followed by normoxia (or hyperoxia) resulting from various environmental factors that may be encountered by pilots (such as rapid acceleration or oxygen supply issues), may lead to brain tissue damage due to oxidative stress (and inflammatory) mechanisms associated with reperfusion injury. In such cases, when the tissue blood supply returns to normal after a period of ischemia or lack of oxygen, the prior hypoxic conditions creates a condition in which the restoration of circulation (reperfusion) results in inflammation and oxidative damage through the induction of oxidative stress, potentially leading to cognitive issues (Carden & Granger, 2000).

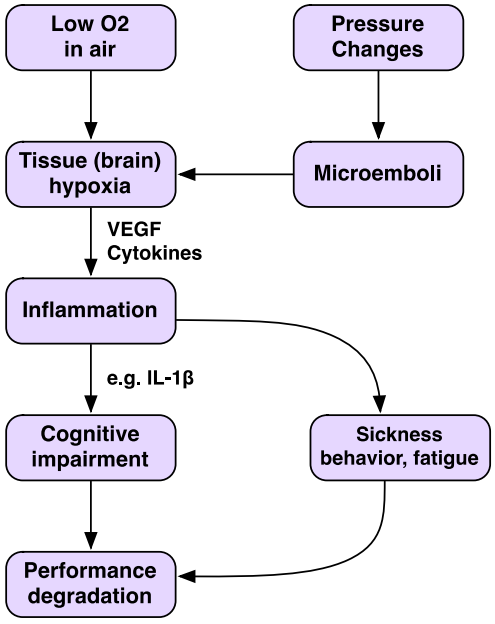

Figure 13. Relation between Brain Tissue Hypoxia, Neuroinflammation and Performance Degradation

Cytokine release following hypoxia has been observed experimentally. For example, Kozak *et al.* (2006) demonstrated that mice exposed for 7 days to hypoxia (11 percent O_2) resulted in significant elevation of plasma IL-6 (see Figure 14), inducing sickness behavior, a set of adaptive responses of the host to severe infections and inflammation. It includes, among others, the thermoregulatory responses such as regulated increase (fever) and/or decrease of body temperature (Tb), decrease of motor activity (lethargy), and loss of appetite (Kozak *et al*., 2006). Such time-course data may ultimately be described by a model that includes HIF-1α – induced gene transcription and further pro-inflammatory processes.

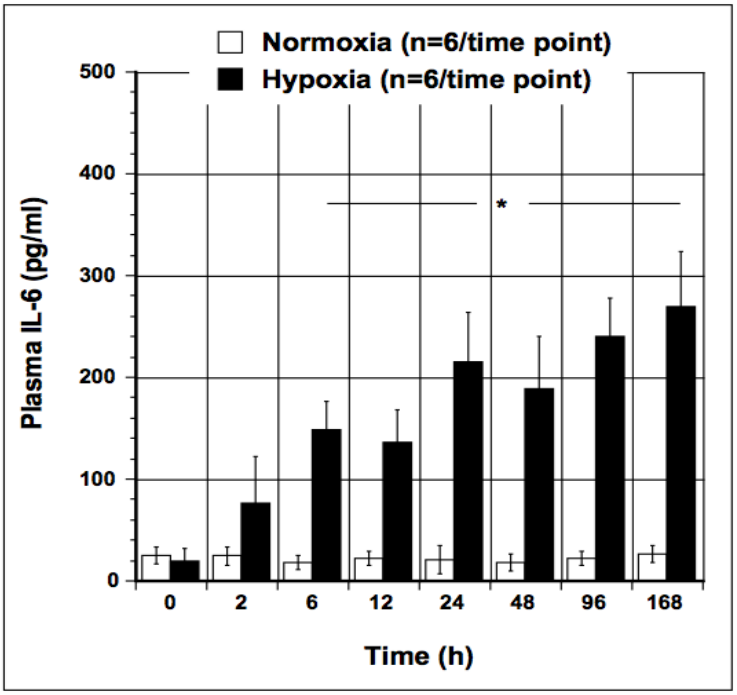

Figure 14. Changes of Plasma IL-6 Levels over Time. Swiss Webster mice were exposed to hypoxia (11 percent O_2; closed bars) and normal air (open bars). Plasma IL-6 levels are expressed in pg/mL and time in hours (h). From Kozak *et al*. (2006).

5.4 Carotid Body and Other Issues

Application of the HIF-1α model to the carotid body is more speculative (see Introduction). However, "hydroxylation of HIF in the presence of O_2 occurs in a few minutes, hence it is conceivable that O_2-dependent hydroxylases could also modulate ion channels and thus participate in the acute responses to hypoxia" (Lopez-Barneo *et al*., 2008). The carotid body response on heart rate, breathing rate, clearly needs to be rapid. Rapid response pathways potentially mediated, at least in part, by the HIF-1α pathway, include nitric oxide synthase (NOS) activation (Jung *et al*., 2000), vasodilation, glucose transport, and metabolism. If we assume that oxygen sensing is again mediated by the intracellular levels of HIF-1α, then we have the scheme outlined in Figure 15.

Transport of HIF-1α to nucleus takes place via microtubules - filamentous intracellular structures that are responsible for various kinds of movements in all eukaryotic cells. Microtubules are involved in nucleic and cell division (chromosome separation in mitosis), organization of intracellular structure, and intracellular transport. Carbonaro *et al*. (2012) showed that HIF-1α protein associates with polymerized microtubules and is transported to the nucleus with the aid of the dynein motor protein. Microtubule-targeting drug (MTD) treatment impaired HIF-1α protein nuclear translocation, which significantly down-regulated HIF transcriptional activity. Understanding of the microtubule-dependent HIF-1α regulation is essential given the importance of HIF-1α in tumor biology, particularly tumor angiogenesis, and the widespread use

of MTDs in clinical oncology (Carbonaro *et al*., 2012). Because of the importance of microtubules in a myriad of other transport processes, particularly regarding transport of receptors and ion channels to membranes in cognition and memory formation, disruption occurring with MTDs (and other stressors) clearly has far-reaching implications. The involvement of microtubules in both hypoxia signaling and cognition also suggests the potential for significant cross-talk between these processes.

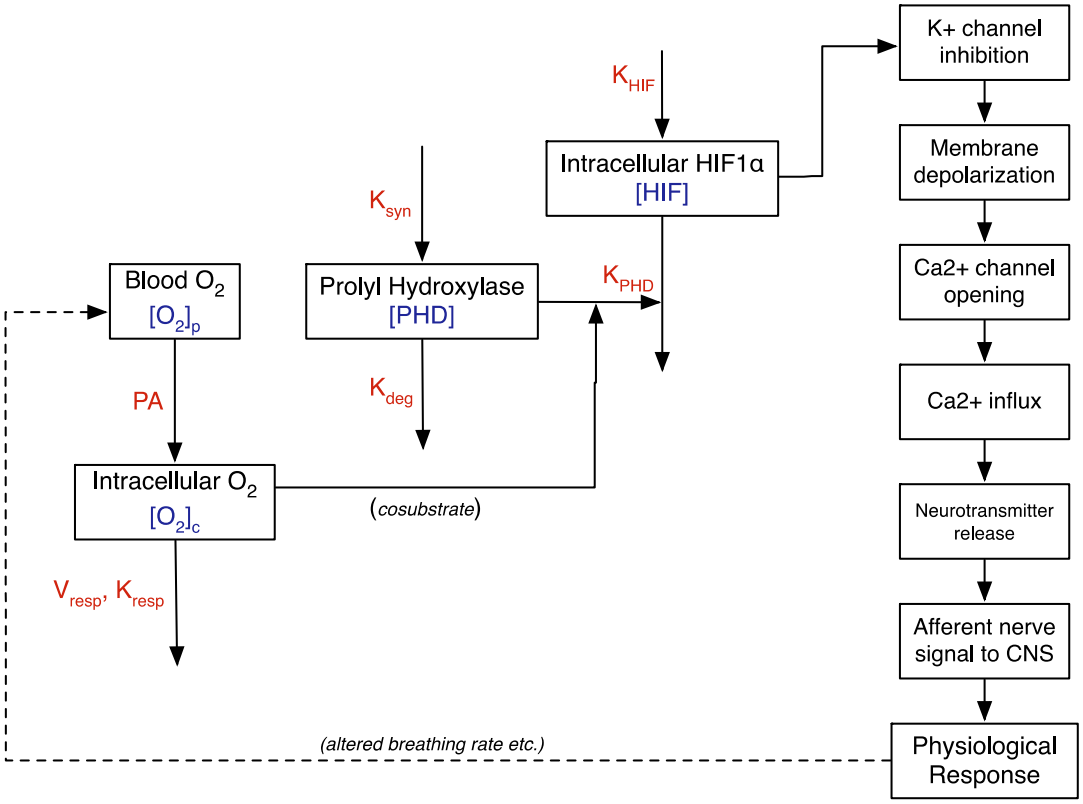

Figure 15. Schematic of a Potential Model for Oxygen Sensing in the Carotid Body

In many cases oxygen delivery issues are concurrent with ambient diverse chemical exposure issues. For example, toluene is a known contamination component that comes through the aircraft's on-board oxygen generation system, and may potentially impact oxygen delivery (Martin *et al.*, 2012). Previous in-house experiments have investigated the effect of altitude on the distribution of toluene in rats by providing a better understanding of how these stressors affect the brain at the cellular and molecular level. Ongoing studies with toluene combined with hypoxia are investigating the effects of altitude, chemical exposure and altered percentage of oxygen on the function of neural cells in the brain by measuring changes in the electrical patterns of brain cells. Toluene also may potentially interact with hemoglobin, altering its binding characteristics and thereby the oxygen carrying capacity of blood (Chushak *et al.*, 2015).

Oxygen delivery to tissues has been significantly studied; the current oxygen transport model is necessarily a simplification of a complex process. Improvements to the oxygen transport model,

based on this extensive literature, could include more dynamic detail, such as a 4-stage binding approach with K_{on} and K_{off} rates. Delivery to brain also depends critically on local cerebral blood flows, which respond to metabolic demands based on brain functional activity. Control of cerebral blood flow is complex and only partially understood. Relevant processes include cerebral pressure autoregulation, which maintains a constant flow despite changing cerebral perfusion pressure. The brain is also able to vary blood flow to match metabolic activity (flow-metabolism coupling). Finally, a network of perivascular nerves also serves to regulate cerebral blood flow (neurogenic regulation) (Peterson *et al*., 2011).

We have treated PHD in the model as a single enzyme – in reality, 3 PHD isoforms have been identified, that contribute to the regulation of HIF-1α (Appelhoff *et al*., 2004). It is hypothesized that their differing cell specific behaviors may lead to flexibility in the HIF-1α response. Once these behaviors are more fully characterized, a more subtle response to hypoxia could be incorporated into the model.

6.0 REFERENCES

Ay, A., & Arnosti, D. N. (2011). Mathematical modeling of gene expression: a guide for the perplexed biologist Critical reviews in biochemistry and molecular biology, 46(2), 137–151. doi:10.3109/10409238.2011.556597

Appelhoff, R. J., Tian, Y.-M., Raval, R. R., Turley, H., Harris, A. L., Pugh, C. W., Ratcliffe, P. J., *et al*. (2004). Differential Function of the Prolyl Hydroxylases PHD1, PHD2, and PHD3 in the Regulation of Hypoxia-inducible Factor. The Journal of biological chemistry, 279(37), 38458–38465. doi:10.1002/jcb.20067

Benson, A. P., Grassie, B., Rossiter, H. B. (2013). A validated model of oxygen uptake and circulatory dynamic interactions at exercise onset in humans. Journal of Applied Physiology, 115, 743-755.

Berne, R.M., Levy, M.N., Koeppen, B.M. and Stanton, B.A. (2004) *Physiology, 5th Edition.* Mosby, St. Louis.

Carbonaro, M., Escuin, D., O'Brate, A., Thadani-Mulero, M., & Giannakakou, P. (2012). Microtubules Regulate Hypoxia-inducible Factor-1α Protein Trafficking and Activity. The Journal of biological chemistry, 287(15), 11859–11869. doi:10.1021/bi962724m

Carden, DL; Granger, DN (Feb 2000). "Pathophysiology of ischaemia-reperfusion injury". The Journal of Pathology. 190 (3): 255–66.

Cavadas, M. A., Nguyen, L. K., & Cheong, A. (2013). Hypoxia-inducible factor (HIF) network: insights from mathematical models Cell communication and signaling: CCS, 11(1), 42. doi:10.1186/1478-811X-11-42

Chavez, J. C., Agani, F., Pichiule, P., & Lamanna, J. C. (2000). Expression of hypoxia-inducible factor-1 alpha in the brain of rats during chronic hypoxia. Journal of applied physiology (Bethesda, MD: 1985), 89, 1937–1942.

Chen, T., He, H. L., & Church, G. M. (1999). Modeling gene expression with differential equations. Pacific Symposium of Bio computing, 1–12.

Cheng, L., Albanese, A., Ursino, M., Chbat, N. W. (2016). An integrated mathematical model of the human cardiopulmonary system: model validation under hypercapnia and hypoxia. Am J Physiol Heart Circ Physiol, 310, H922-H937.

Chushak, Y. G., Chapleau, R. R., Frey, J. S., Mauzy, C. A., Gearhart, J. M. (2015) Identifying potential protein targets for toluene using molecular similarity search, *in silico* docking and *in vitro* validation. Toxicol. Res. 4, 519-526.

Collins, J.-A., Rudenski, A., Gibson, J., Howard, L., & O'Driscoll, R. (2015). Relating oxygen partial pressure, saturation and content: the haemoglobin–oxygen dissociation curve. Breathe, 11(3), 194–201. doi:10.1183/20734735.001415

Davies, Melissa (2002-04-09). "The Neuron: size comparison". Neuroscience: A journey through the brain. Retrieved 2009-06-20.

Dayan, F., Monticelli, M., Pouyssegur, J., & Pécou, E. (2009). Gene regulation in response to graded hypoxia: The non-redundant roles of the oxygen sensors PHD and FIH in the HIF pathway. Journal of theoretical biology, 1–26. Elsevier. doi:10.1016/j.jtbi.2009.03.009

Dijkhuizen, P., A. Buursma, T. M. E. Fongers, A. M. Gerding, B. Oeseburg, W. G. Zijlstra. The oxygen binding capacity of human haemoglobin. Hüfner's factor redetermined. Pflügers Archiv, 369, 223–231, 1977.

Dings J, Meixensberger J, Jäger A, *et al*. Clinical experience with 118 brain tissue oxygen partial pressure catheter probes. Neurosurgery. 1998; 43: 1082–95.

Duffin, J., Mohan, R. M., Vasiliou, P., Stephenson, R., Mahamed, S. (2000). A model of the chemoreflex control of breathing in humans: model parameters and measurement. Respiratory Physiology, 120, 13-26.

Grodins, F. S., Buell, J., Bart, A. (1967). Mathematical analysis and digital simulation of the respiratory control system. J. Appl. Physiol., 22(2), 260-276.

Hirsilä, M., Koivunen, P., Günzler, V., Kivirikko, K. I., & Myllyharju, J. (2003). Characterization of the human prolyl 4-hydroxylases that modify the hypoxia-inducible factor The Journal of biological chemistry, 278(33), 30772–30780. doi:10.1074/jbc.M304982200

Johnson, P. C., Vandegriff, K., Tsai, A. G., & Intaglietta, M. (2005). Effect of acute hypoxia on microcirculatory and tissue oxygen levels in rat cremaster muscle Journal of applied physiology (Bethesda, MD: 1985), 98(4), 1177–1184. doi:10.1152/japplphysiol.00591.2004

Jung, F., Palmer, L. A., Zhou, N., & Johns, R. A. (2000). Hypoxic regulation of inducible nitric oxide synthase via hypoxia inducible factor-1 in cardiac myocytes Circulation research, 86(3), 319–325.

Kaelin, W. G., Jr., & Ratcliffe, P. J. (2008). Oxygen Sensing by Metazoans: The Central Role of the HIF Hydroxylase Pathway. Molecular Cell, 30(4), 393–402. doi:10.1016/j.molcel.2008.04.009

Kline, D. D., Peng, Y., Manalo, D. J., Semenza, G. L., Prabhakar, N. R. (2002) Defective carotid body function and impaired ventilatory responses to chronic hypoxia in mice partially deficient for hypoxia-inducible factor 1α. Proc. Natl. Acad. Sci. USA, 99, 821–826

Kohn, K. W. (2004). Properties of Switch-like Bioregulatory Networks Studied by Simulation of the Hypoxia Response Control System. Molecular biology of the cell, 15(7), 3042–3052. doi:10.1091/mbc.E03-12-0897

Kooner P, Maini P, Gavaghan D: Mathematical modelling of the HIF-1 mediated hypoxic response in tumours. In , Proceedings of the 2005 International Symposium on Mathematical & Computational Biology BIOMAT 2005Edited by Mondaini R, Dilao R. Rio de Janeiro: E-papers Servicos Editoriais Ltda; 2006:261–316.

Koivunen, P., Tiainen, P., Hyvärinen, J., Williams, K. E., Sormunen, R., Klaus, S. J., Kivirikko, K. I., *et al*. (2007). An endoplasmic reticulum transmembrane prolyl 4-hydroxylase is

induced by hypoxia and acts on hypoxia-inducible factor α The Journal of biological chemistry, 282(42), 30544–30552. doi:10.1074/jbc.M704988200
Kozak, W., Wrotek, S., & Walentynowicz, K. (2006). Hypoxia-induced sickness behaviour Journal of physiology and pharmacology: an official journal of the Polish Physiological Society, 57 Suppl 8, 35–50.
LaManna, J. C., Chavez, J. C., Pichiule, P. (2004). Structural and functional adaptation to hypoxia in the rat brain. J. Exper. Biol. 207(Pt 18), 3163–3169
López-Barneo, J., Ortega-Sáenz, P., Pardal, R., Pascual, A., & Piruat, J. I. (2008). Carotid body oxygen sensing The European respiratory journal: official journal of the European Society for Clinical Respiratory Physiology, 32(5), 1386–1398. doi:10.1183/09031936.00056408
Lynch, M. A. (2010). Age-related neuroinflammatory changes negatively impact on neuronal function Frontiers in aging neuroscience, 1, 6. doi:10.3389/neuro.24.006.2009
Martin, G., Muellner, G., Anderson, J., Brinkley, J., Delaney, L., Demitry, P., Moore, D, Moorman, T. (2012). Report on Aircraft Oxygen Generation. Washington, D.C.: United States Air Force Scientific Advisory Board. SAB-TR-11-04, 1 February 2012.
McGuire, S. A., Tate, D. F., Wood, J., Sladky, J. H., McDonald, K., Sherman, P. M., Kawano, E. S., *et al*. (2014). Lower neurocognitive function in U-2 pilots: Relationship to white matter hyperintensities Neurology, 83(7), 638–645. doi:10.1212/WNL.0000000000000694
McGuire, S., Sherman, P., Profenna, L., Grogan, P., Sladky, J., Brown, A., Robinson, A., *et al*. (2013). White matter hyperintensities on MRI in high-altitude U-2 pilots Neurology, 81(8), 729–735. doi:10.1212/WNL.0b013e3182a1ab12
McGuire, S. A., Sherman, P. M., Wijtenburg, S. A., Rowland, L. M., Grogan, P. M., Sladky, J. H., Robinson, A. Y., *et al*. (2014b). White matter hyperintensities and hypobaric exposure. Annals of neurology, 76(5), 719–726. doi:10.1002/ana.24264
Nguyen, L. K., Cavadas, M. A. S., Scholz, C. C., Fitzpatrick, S. F., Bruning, U., Cummins, E. P., Tambuwala, M. M., *et al*. (2013). A dynamic model of the hypoxia-inducible factor 1α (HIF-1α) network Journal of cell science, 126(Pt 6), 1454–1463. doi:10.1242/jcs.119974
Peng, Y., Yuan, G., Ramakrishnan, D., Sharma, S. D., Bosch-Marcé, M., Kumar, G. K., Semenza, G. L., Prabhakar, N. R. (2006) Heterozygous HIF-1α deficiency impairs carotid body-mediated systemic responses and reactive oxygen species generation in mice exposed to intermittent hypoxia. J. Physiol. 577, 705–716.
Peterson, E. C., Wang, Z., & Britz, G. (2011). Regulation of Cerebral Blood Flow. International Journal of Vascular Medicine, 2011(1), 1–8. doi:10.1038/24388
Prabhakar, N. R. (2013). Sensing hypoxia: physiology, genetics and epigenetics The Journal of Physiology, 591(Pt 9), 2245–2257. doi:10.1113/jphysiol.2012.247759
Qutub, A. A. (2006). A computational model of intracellular oxygen sensing by hypoxia-inducible factor HIF1. Journal of cell science, 119(16), 3467–3480. doi:10.1242/jcs.03087
Qutub, A. A., & Popel, A. S. (2007). Three autocrine feedback loops determine HIF1α expression in chronic hypoxia. Biochimica et Biophysica Acta (BBA) - Molecular Cell Research, 1773(10), 1511–1525. doi:10.1016/j.bbamcr.2007.07.004
Qutub, A. A., Mac Gabhann, F., Karagiannis, E. D., Vempati, P., & Popel, A. S. (2009). Multiscale models of angiogenesis IEEE engineering in medicine and biology magazine: the quarterly magazine of the Engineering in Medicine & Biology Society, 28(2), 14–31. doi:10.1109/MEMB.2009.931791
R Core Team (2016). R: A Language and Environment for Statistical Computing, https://www.R-project.org

Robinson *et al*. (2016). Technical Report AFRL-RH-WP-TR-2016-0086. *Host - HIF-1α Pathway and Hypoxia: In Vitro Studies and Mathematical Model.*

Schmierer, B., Novak, B., & Schofield, C. J. (2010). Hypoxia-dependent sequestration of an oxygen sensor by a widespread structural motif can shape the hypoxic response - a predictive kinetic model. BMC Systems Biology, 4(1), 139. BioMed Central Ltd. doi:10.1186/1752-0509-4-139

Schoch, H. J., Fischer, S., & Marti, H. H. (2002). Hypoxia-induced vascular endothelial growth factor expression causes vascular leakage in the brain. Brain: a journal of neurology, 125(Pt 11), 2549–2557.

Semenza, G. L. (2004). Hydroxylation of HIF-1: oxygen sensing at the molecular level Physiology (Bethesda, MD), 19, 176–182.

Sinski M, Lewandowski J, Przybylski J, Zalewski P, Symonides B, Abramczyk P, Gaciong Z. (2014). Deactivation of carotid body chemoreceptors by hyperoxia decreases blood pressure in hypertensive patients. Hypertens Res. 2014 Sep; 37(9):858-62. doi: 10.1038/hr.2014.91.

Topor, Z. L., Pawlicki, M., & Remmers, J. E. (2004). A computational model of the human respiratory control system: responses to hypoxia and hypercapnia Annals of biomedical engineering, 32(11), 1530–1545.

Vezzani, A. (2005). VEGF and seizures. Current Literature in Basic Science, 1–3.

Ward, S. A. (2007). Ventilatory control in humans: constraints and limitations. Experimental Physiology, 92.2, 357-366.

Wolf, B. W., Garner, R. P. (2007). A mathematical model of human respiration at altitude. Annals of Biomedical Engineering, 35(11), 2003-3022.

Yu, Y., Wang, G., Simha, R., Peng, W., Turano, F., & Zeng, C. (2007). Pathway Switching Explains the Sharp Response Characteristic of Hypoxia Response Network. PLoS computational biology, 3(8), e171.

Yucel, M. A., & Kurnaz, I. A. (2007). An *in silico* model for HIF-α regulation and hypoxia response in tumor cells. Biotechnology and bioengineering, 97(3), 588–600. doi:10.3934/dcdsb.2004.4.267

APPENDIX A. MODEL CODE: COMBINED OXYGEN TRANSPORT AND HIF-1A MODEL

Note that the HIF-1α model was originally encoded in Berkeley Madonna software and presented in a previous Technical Report (Robinson *et al*., 2016)

```
# O2 transport and HIF response model
# Version 7.1
# 8 September 2017
# C. Eric Hack and Peter J. Robinson
# Kinetic model of oxygen delivery to the brain and HIF1a signaling.

# lines beginning with '#' are comments, and not executed

# clean the workspace
rm(list=ls())

# load the solver
library(deSolve)


#########################################################################
# Constants

#-------Initial conditions for the amounts
ATB0 <- 4
ATT0 <- 43
ABrB0 <- 0.01
ABrT0 <- 1
HIF0 <- 1e-9
HIFN0 <- 1e-14
TC0 <- 5.3e-11

#-------Chemical parameters
     MW <- 32.0         # Molecular weight (g/mole) of O2
     MW2 <- 44.0  # Molecular weight (g/mole) of metabolite (CO2)

#-------Physiological parameters

    QPC <- 14.          # Alveolar ventilation rate (L/hr)
    QCC <- 14.          # Cardiac output (L/hr)
    QBrC <- 0.10  # Fractional blood flow to brain (L/hr; Gerlowski and Jain,
1983)
    QTC <- 0.9          # Fractional blood flow to rest of body (L/hr)

     BW <- 70           # Body weight (kg)
   VBrC <- 0.02         # Fraction brain tissue (kg or L)
  VBrBC <- 0.05         # Fraction of brain that is blood
    VTC <- 0.89         # Fraction rest of body tissue (kg or L; total ~91%
perfused)
   VBld <- 0.075  # Fraction blood in while body
   VTBC <- VBld - VBrC*VBrBC  # Fraction of rest of body that is blood

    # Partition coefficients
    PB <- 0.03          # Blood:air
   PBr <- 1       # Brain:blood
    PT <- 1       # Rest of body tissues:blood
  PABr <- 0.01          # Permeability X Area cross product between brain
blood and brain tissue
   PAT <- 1.01          # Permeability X Area cross product between tissue
blood and tissue cells
```

```
    # Metabolism parameters
    VMAXBrC <- 1  # Brain Maximum rate of metabolism (mg/hr)
    VMAXTC <- 1         # Tissue Maximum rate of metabolism (mg/hr)
    KM <- 1       # Half-max concentration (mg/L); not scaled by BW

#-------Inhalation exposure parameters
      P <- 1            # Pressure (atm)
  PmmHg <- P*760  # Pressure (mmHg)
    FO2 <- 0.21         # Fraction O2 in outside air
   PH2O <- 47           # Water vapor pressure in alveolus (mmHg)
  humid <- (PmmHg - PH2O)/760 # Note that this is about 6% reduction from 760
mmHg, and agrees with Karius.
                  #  (Karius DR, "Respiratory Adaptations in Health and
Disease: Calculating the Alveolar
                  #  Oxygen & the A-a O2 gradient", a Kansas City University
of Medicine and Biosciences online lecture).
     CC <- FALSE  # Default to open chamber
  NRATS <- 3.           # Number of rats (for closed chamber)
    KLC <- 0.           # First order loss from closed chamber (/hr)
   VCHC <- 9.1          # Volume of closed chamber (L)
  TCHNG <- 12.0         # Length of inhalation exposure (hrs)

#-------Timing commands
#? How to incorporate multiple changes in exposure in R?
#? Are the good, built-in forcing functions, like step functions?
  TSTOP <- 24.0  # Length of experiment (hrs)
 POINTS <- 100   # Number of points in plot
   CINT <- TSTOP/POINTS  # Communication interval (for output, hrs)

#-------Uptake of inhaled O2 based on Hgb saturation curve
# The hbg binding parameters are set in the Fit.CB.R script.
#   Retained here for documentation purposes.
   Bmax <- 1      # fraction Hgb occupied by O2
     KD <- 42     # mmHg
      n <- 2.4    # Hill coefficient for O2 binding to Hgb
    hgb <- 150      # g Hgb / L blood

#-------Ideal gas law parameters for conversion between mL O2 and mg O2 (CA)
# The conditions are for STPD, since the mL represents what would be the
volume at STPD.
     R <- 0.082056      # Universal gas constant (L*atm/K/mol)
  Temp <- 273.15  # Standard temperature (K)
 BTemp <- Temp + 37     # Body temperature (K)

#-------Conversion factor for STPD to BTPS
  StoB <- (760)/(PmmHg - PH2O) * (BTemp)/(Temp)       # = 863/(PmmHg - 47)

#-------Dummy parameter for CA and CV extraction
  kbig <- 1.0e9

# Get relationship between CF (free) and CB (bound).
  source("Fit.CB.R")
# The parameters are assigned by the script file.
#  Bmax <- coef(fit)[1]
#  KD <- coef(fit)[2]
#  n <- coef(fit)[3]

#-------HIF submodel-specific parameters
# most parameters are from Nguyen et al. (2013)
Kphd <- 162                   # /hr
Tmax <- 1e-3/1e3*3600               # uM/hr
KT <- 1                             # uM
Khif <- 1.8e-2                      # uM/hr
Kbm <- 32.4                   # /hr
```

```
HRE <-1                                 # Kbm*HRE = 32.4/hr
KdegN <- 1                        # /hr
Ktc <- 0.36                       # /hr
PHD <- 5000                       # uM
KmHIF <- 0.1                            # uM
KmO2 <- 250                       # uM

#-------Modify the inhaled O2 fractions and duration (change times are
calculated)
  # O2 fractions
  Oxy <- c(0.21, 0.105, 0.21, 0.21)
  # Change times and durations
  Dur <- c(1, 6, 1, Inf)
  tau <- c(0, Dur[1] + Dur[2], sum(Dur[1:3]))

#########################################################################
# Modify constants

  # Source a file with modifications to the default constant parameter values.
  # This needs to be done before calculations based on the constants.
  # For example, load a rat or human physiological parameter file,
  #  or change the dosing parameters, or change the chemical.

  # Can have multiple R scripts called here.

  #BUT BE CAREFUL OF THE ORDER!
  #(that is, when changing the same parameter in multiple files)


  # Set species-specific parameters
  source("rat.R") # sets BW to 0.3, VFC to 0.09
  #source("human.R")

  # Set chemical-specific parameters
  #source("Styrene.R")  # placeholder for future addition of other chemicals

  # Set exposure scenario
  source("hypoxia2.R")  # load a particular hypoxic event
  #source("modify.R")   # placeholder for other parameter modifications
  #source("johnson.R")  # simulate the Johnson study

#########################################################################
# Scaled or Adjusted or Calculated parameters

  # convert from fraction O2 in atmosphere, and decrease for humidification.
   CONC <- P*FO2*1.0e6*humid  # Inhaled concentration (ppm)

if (CC) { # Closed chamber simulation
      RATS <- NRATS
      KL <- KLC
} else {
      RATS <- 0.
      KL <- 0. # (Turn off chamber losses so concentration remains constant)
}

VCH <- VCHC-RATS*BW        # Net chamber volume (L)
AI0 <- CONC*VCH*MW/24450.  # Initial amount in chamber (mg)



#------Allometric scaling
# Flows (blood and respiration)
QC <- QCC*BW**0.74# Cardiac output (L/hr)
QP <- QPC*BW**0.74      # Alveolar ventilation (L/hr)
```

```
QBr <- QBrC*QC          # Brain blood flow (L/hr)
QT <- QTC*QC            # Rest of tissues blood flow (L/hr)

# Tissue Volumes
VBr <- VBrC*BW          # Brain total (L)
VBrB <- VBrBC*VBr # Brain blood (L)
VBrT <- VBr - VBrB      # Brain tissue (L)
VT <- VTC*BW            # Rest of tissues (L)
VTB <- VTBC*VT          # Tissue blood (L)
VTT <- VT - VTB         # Tissue tissue/cells (L)

# Metabolism
VMAXBr <- VMAXBrC*BW**0.7     # Maximal rate (mg/hr)
VMAXT <- VMAXTC*BW**0.7       # Maximal rate (mg/hr)

# Conversion factors
nMps2mgph <- VBrT*3600*MW/1e6 # convert nM/s to mg/hr
# nMps2mgph needed to use the HIF-PHD-O2 equation in the brain tissue rate eqn.


######################################################################
# Define the model/system of ODEs

dynamic <- function (times, state, parms) {
 with(as.list(c(state, parms)), {

#----DYNAMIC:  Things that change with time go in this function definition

#----Compartments
#     Brain tissue
#     Brain blood
#     Alveolar gas exchange (CI, CA, CX)
#     Arterial blood Hgb (CAF, CAB)
#     Rest of body tissue (cells)
#     Rest of body blood

#----Inhalation
   # idx is exposure index variable
   idx <- 0
   len <- length(tau)
   for (i in 1:len) { idx <- idx + as.numeric(times >= tau[i]) }
   frax <- Oxy[idx]/Oxy[1]

CIZONE <- as.numeric(CC | (times < TCHNG)) # 0 if CC=False and t>=TCHNG, 1
otherwise
   CI <- AI/VCH*CIZONE*frax               # Concentration in alveolar air
(mg/L)
   CP <- CI*24450./MW                 # Alveolar Air Concentration (ppm)

#----Body, or Tissues (T)
   CTT <- ATT/VTT # tissue/cells
   CVT <- ATB/VTB # tissue blood

#----Brain
  CBrT <- ABrT/VBrT
  CVBr <- ABrB/VBrB

#----CV = Mixed venous blood concentration (mg/L)
   CV <- (QT*CVT + QBr*CVBr)/QC

#----PAO2 = alveolar PO2 (mmHg)
  PAO2 <- P*760*Oxy[idx]*humid      # alveolar O2 (mmHg)

#----CA = Concentration in arterial blood (mg/L)
```

```
# Implicit solve for CAF.  Find the zero of the function using uniroot().
  f <- function(x) {QP*(CI - x/PB) + QC*(CV - Bmax*x**n/(KD**n + x**n) - x)}
  soln <- uniroot(f, c(0,300))
  CAF <- soln$root

# Now compute bound O2
  CAB <- Bmax*CAF**n/(KD**n + CAF**n)

# Total arterial O2
  CA <- CAF + CAB

# Exhaled O2
   CX <- CAF/PB                          # Concentration in exhaled air (mg/L)
   CXPPM <- (0.7*CX+0.3*CI)*24450./MW    # Concentration (ppm), 30% dead space
assumed

#----A = dummy for CA
   dA <- kbig*(CA - A)

#----V = dummy for CV
   dV <- kbig*(CV - V)

#----AI = Amount in inhaled air (mg/L)
    dAI <- RATS*QP*(CAF/PB-CI) - (KL*AI) # Rate of change in air amount
(mg/hr)
    dAInh <- QP*CI                       # Rate inhaled (mg/hr)

#----AX = Amount exhaled (mg)
    dAX <- QP*CX                         # Rate exhaled (mg/hr)

#----ABr = Amount in brain blood (mg)
    brup <- PABr*(CVBr - CBrT/PBr)  # oxygen diffusion from brain blood to
tissue (mg/hr)
    dABrB <- QBr*(CA - CVBr) - brup

#----AT = Amount tissues in rest of body (mg)
    dATB <- QT*(CA - CVT) - PAT*(CVT - CTT/PT)  # tissue blood
    dATT <- PAT*(CVT - CTT/PT) - VMAXT*CTT/(KM + CTT)

#----AM = Amount metabolized in brain and rest of body (mg)
    brmet <- VMAXBr*CBrT/(KM + CBrT)
    tmet <- VMAXT*CTT/(KM + CTT)
    hifmet <- Kphd*PHD*HIF*CBrT/((HIF+KmHIF)*(CBrT+KmO2))
    dAM <- brmet + tmet + hifmet    # total metabolism


#----HIF1a submodel
    # Oxygen diffuses in from blood and is removed from cytosol via
respiration and hydroxylation of HIF
    dABrT <- brup - brmet - hifmet*nMps2mgph          # mg/hr
    # HIF is synthesized, and removed from cytosol by hydroxylation and
transport to nucleus
    hiftrans <- Tmax*HIF/(HIF+KT)               # uM/hr
    dHIF <- Khif - hifmet - hiftrans                  # uM/hr

    # HIF is removed from nucleus by degradation and binding to hypoxia
responsive element (HRE)
    dHIFN <- hiftrans - KdegN*HIFN - Kbm*HIFN*HRE     # uM/hr

    # Transcription signal (TC) creation by binding of HIF to HRE, and
degradation
    dTC <- Kbm*HIFN*HRE - Ktc*TC                # uM/hr
```

```
#----model function must return a list for the ode solver
    return(list(c(dAI, dAInh, dAX, dABrB, dATB, dATT, dAM, dABrT, dHIF, dHIFN,
dTC, dA, dV)))

})
}


######################################################################
# Integration

# Parameters for integrator
# Using global parameters for now,
#  so parms is a dummy to satisfy the input requirements of our derivative
function.
parms <- 1

# States
state <- c(AI = AI0,
           AInh = 0,
           AX = 0,
           ABrB = ABrB0,
         ATB = ATB0,
           ATT = ATT0,
           AM = 0,
         ABrT = ABrT0,
         HIF = HIF0,
         HIFN = HIFN0,
         TC = TC0,
         A = 200,
         V = 200)

# Integration times
times <- seq(0, TSTOP, by = CINT)

# Call the integrator
#out <- ode(y = state, times = times, func = dynamic, parms = parms,
atol=1.0e-12, rtol=1.0e-9)
out <- ode(y = state, times = times, func = dynamic, parms = parms)
y <- as.data.frame(out)



######################################################################
#----Mass balance equations
#----TMASS = total mass stored (mg)
    ABr <- out[,"ABrT"] + out[,"ABrB"]
    AT <- out[,"ATT"] + out[,"ATB"]
    TMASS <- ABr + AT

    TMASS0 <- ABrB0 + ABrT0 + ATB0 + ATT0

#----OUT = amount removed by metabolism and exhalation (mg)
    OUT <- out[,"AM"] + out[,"AX"]

#----DOSEIN = Amount absorbed (mg)
    DOSEIN <- out[,"AInh"]

#----MASSBAL = mass balance = in - out - stored
    MASSBAL <- TMASS0 + DOSEIN - OUT - TMASS
    last <- MASSBAL[length(MASSBAL)]
    names(last) <- "Mass Balance (mg)"
    print(last)
```

```
    mb <- rbind(times, rbind(TMASS0, rbind(DOSEIN, rbind(OUT, rbind(TMASS,
MASSBAL)))))
#     View(mb)


######################################################################
# Plotting routines

source("plotrunWITHburnin.R")
```

APPENDIX B. SUPPORTING R SCRIPTS

hypoxia2.R

```
# Modify constants to simulate hypoxia scenario 2

# Changing oxygen in atmosphere
# Start with fraction O2 (FO2) = 0.21.
# After 6 hour burn in, reduce FO2 to 33% or 0.07, for 2 hours.
# At 8 hours, return to baseline FO2 = 0.21.

print("Sourcing hypoxia2.R")

# Change simulation time, oxygen fractions, and change times

TSTOP <- 12
POINTS <- 120
CINT <- TSTOP / POINTS

# First, turn off the TCHNG variable (controlling with others)
TCHNG <- Inf

# O2 fractions
Oxy <- c(0.21, 0.07, 0.21, 0.21)

# Change times and durations
Dur <- c(6, 2, 6, Inf)
tau <- c(0, Dur[1], Dur[1] + Dur[2], sum(Dur[1:3]))
```

Fit.CB.R

```
# Fit.CB.R
# Get relationship between CF (free) and CB (bound).

print("Sourcing Fit.CB.R")

Pa <- seq(0,150,5)
source('~/Documents/2017 Projects/O2/working/Fit.SaO2.orig.R')
S <- function(p) { p**n/(KD**n + p**n) }

caf <- function(p) { 0.003*p }
cab <- function(p) { 1.39*150*S(p) }
b <- cab(Pa)
e <- rnorm(length(b), 0, 0.1)
b <- b + e
f <- caf(Pa)

plot(f, b)

bmax0 <- 200
kd0 <- 0.15
n0 <- 2.5
guess <- bmax0*f**n0/(kd0**n0 + f**n0)
lines(f, guess)

# Have to add a little error (e) or the nls algorithm fails.
# So, run multiple times and average the resulting parameters.
top <- 100
bsum <- 0
ksum <- 0
```

```
nsum <- 0
for (idx in 1:top) {
  fit <- nls(b ~ Bmax*f**n/(KD**n + f**n), start=list(Bmax=bmax0, KD=kd0,
n=n0))

  bsum <- bsum + coef(fit)[1]
  ksum <- ksum + coef(fit)[2]
  nsum <- nsum + coef(fit)[3]

  b <- cab(Pa)
  e <- rnorm(length(b), 0, 0.1)
  b <- b + e

}

summary(fit)
pred <- predict(fit)
lines(f, pred)

Bmax <- bsum/top
KD <- ksum/top
n <- nsum/top
```

plotrunWITHburnin.R

```
# calculate burn-in time
end <- POINTS
begin <- floor(POINTS*0.05)

CT <- out[begin:end,"ATT"]/VTT
CTB <- out[begin:end,"ATB"]/VTB
CBr <- out[begin:end,"ABrT"]/VBrT
CBrB <- out[begin:end,"ABrB"]/VBrB
PctT <- out[begin:end,"ATT"]/ATT0*100
PctBr <- out[begin:end,"ABrT"]/ABrT0*100
t <- out[begin:end,"time"]
tau <- t - t[1]

#plot(t, PctT, type="l", xlab="Time (hr)", ylab="Blood Percent Oxygen")
#plot(t, PctBr, type="l", xlab="Time (hr)", ylab="Brain Percent Oxygen")
plot(tau, out[begin:end,"A"], type="l", xlab="Time (hr)", ylab="Arterial Blood
Concentration (mg/L)")
plot(tau, out[begin:end,"V"], type="l", xlab="Time (hr)", ylab="Venous Blood
Concentration (mg/L)")
plot(tau, CT, type="l", xlab="Time (hr)", ylab="Body/Tissue Oxygen
Concentration (mg/L)")
plot(tau, CTB, type="l", xlab="Time (hr)", ylab="Body/Tissue Blood Oxygen
Concentration (mg/L)")
plot(tau, CBr, type="l", xlab="Time (hr)", ylab="Brain Oxygen Concentration
(mg/L)")
plot(tau, CBrB, type="l", xlab="Time (hr)", ylab="Brain Blood Oxygen
Concentration (mg/L)")
plot(tau, out[begin:end,"HIF"], type="l", ylab="HIF")
plot(tau, out[begin:end,"HIFN"], type="l", ylab="HIFN")
plot(tau, out[begin:end,"TC"], type="l", ylab="TC")
```

APPENDIX C. MODEL PARAMETERS

Q_c	Cardiac output (total blood flow)
Q_P	Pulmonary blood flow
Q_{Br}	Brain blood flow
C_A	Arterial blood oxygen concentration ($=C_F + C_B$)
C_F	Free oxygen concentration in blood
C_B	Bound oxygen concentration in blood
C_V	Venous blood O_2 concentration
C_F	Free oxygen concentration in blood
C_I	Inhaled air O_2 concentration (alveolar)
C_X	Exhaled air O_2 concentration
C_{vBr}	O_2 blood (venous) concentration leaving brain
V_c	Brain intracellular compartment volume
V_n	Brain nuclear compartment volume
A	Amount of O_2 in arterial blood
$A_{Br,T}$, $C_{Br,T}$	Amount and concentration of O_2 in brain intracellular compartment
VMax, KM	Michaelis-Menten parameters for O_2 metabolism
$VMax_{Br}$, V_{resp}, K_{resp}	Michaelis-Menten parameters for O_2 metabolism in brain
PA	Permeability-surface area product for O_2 uptake into brain
P_{Br}	Blood-brain partition coefficient for O_2
PB	Air/blood oxygen partition coefficient
Bmax, KD, n	Hill coefficients for O_2 hemoglobin binding
Hgb	Amount of hemoglobin
PaO2	Partial pressure of O_2 in blood
SaO2	Fraction saturation of hemoglobin
K_{PHD}	PHD-dependent degradation rate constant for HIF-1α in the cytosol
K_{mHIF}, K_{mO2}	HIF-1α and O_2 half-saturation constants for PHD-dependent degradation rate constant for HIF-1α in the cytosol
K_{HIF}	Zero order synthesis rate of HIF-1α in the cytosol
T_{max}, K_T	Maximum rate and half-saturation concentration for transport of HIF-1α from cytosol to nucleus
K^n_{deg}	Degradation rate of HIF-1α in the nucleus
K_{bm}	Rate constant for binding of HIF-1α with hypoxia responsive element (HRE) on the DNA
K_{tc}	Spontaneous decay rate of the transcription signal TC
F	Oxygen unit conversion factor (nM/s to mg/hr)

LIST OF ACRONYMS

BSA	bovine serum albumin
CB	carotid body
CBP	cAMP response element binding (CREB) protein
COHb	carboxyhaemoglobin
2,3-DPG	2,3-diphosphoglycerate
ELISA	enzyme-linked immunosorbent assay
FIH	factor inhibiting hypoxia inducing factor
Hb	hemaglobin
HIF	hypoxia inducing factor
HIFN	hypoxia inducing factor in the nucleus
HRE	hypoxia responsive element
IHC	Immunohistochemical (staining)
OBOGS	on-board oxygen generation system
ODE	ordinary differential equation
PA	permeability area cross product
PBPK	physiologically-based pharmacokinetic (model)
PHD	prolyl hydroxylase
pO_2	partial pressure of oxygen (mmHg)
SS	steady-state
TAD	transactivation domain
TC	transcription signal
VHL	von Hippel-Lindau tumor suppressor protein
VEGF	vascular endothelial growth factor
WMH	white matter hyperintensities